Flux tubes, magnetic reconnection and turbulence in the solar wind

Z.Vörös[1]

T. Zaqarashvili[1], J. Sasunov[1], R. Bruno[2], G. Consolini[2]

Y. Narita[1], I. Zheliazkov[3], STORM team

Project support: EU-FP7-STORM-313038 & FWF P26181-N27

1. Space Research Institute, Austrian Acad. Sciences, Graz, Austria
2. INAF-IAPS, Rome, Italy
3. Faculty of Physics, Sofia University, Bulgaria

Outline

- Turbulence statistics: PDFs
- Turbulence, intermittency and structures
- Reconnection outflow generated turbulence
- Flux tubes within reconnection outflows
- Unstable twisted flux tubes

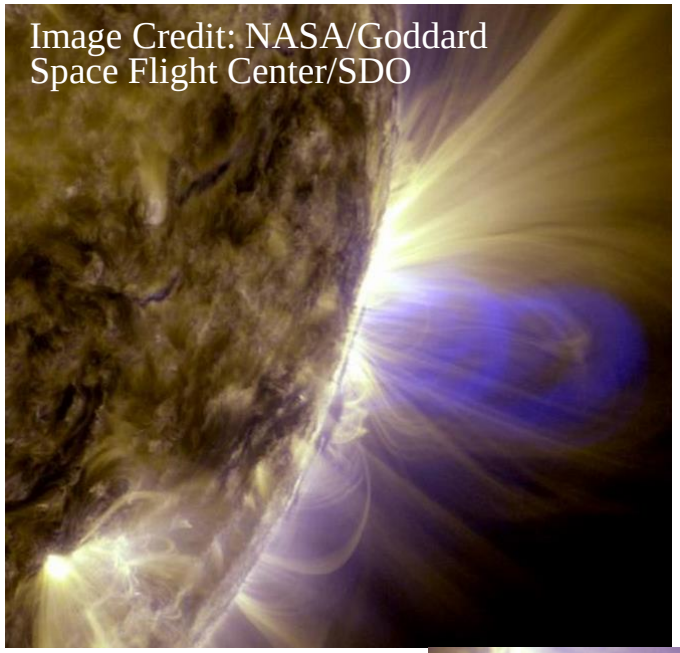
Image Credit: NASA/Goddard Space Flight Center/SDO

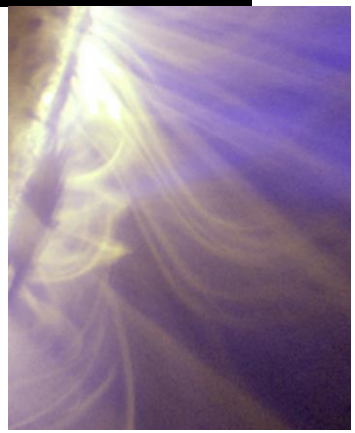


Mamaia beach, 9.9.2015

Intermittency in neutral fluids

"Intermittency is the non-uniform distribution of eddy formations in a stream. The modulus or the square of the vortex field, the energy dissipation velocity or related quantities quadratic in the gradients of velocity and temperature (of the concentration of passive admixture) may serve as indicators." (Novikov, 1971)

Leonardo

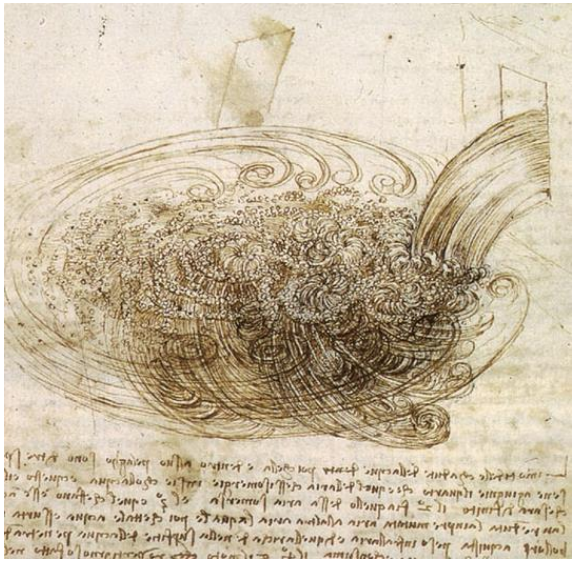

Frisch, 1995

e.g. Jimenez et al., 1993

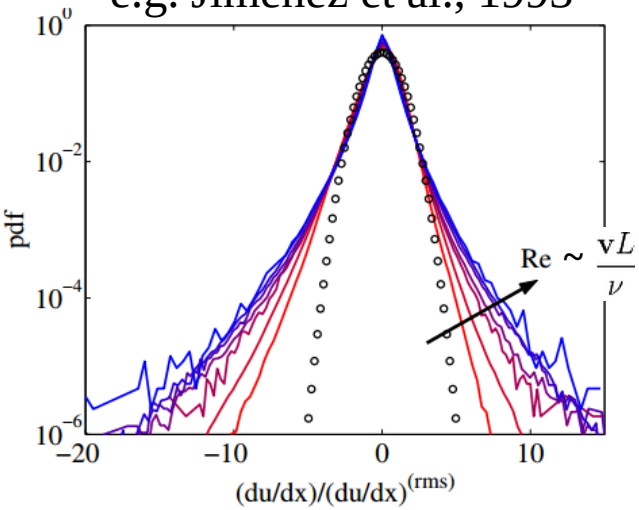

PDFs: strong gradients (long tails) develop when the Re number increases.
Spectra: High Re number turbulence has a wide range of scales.

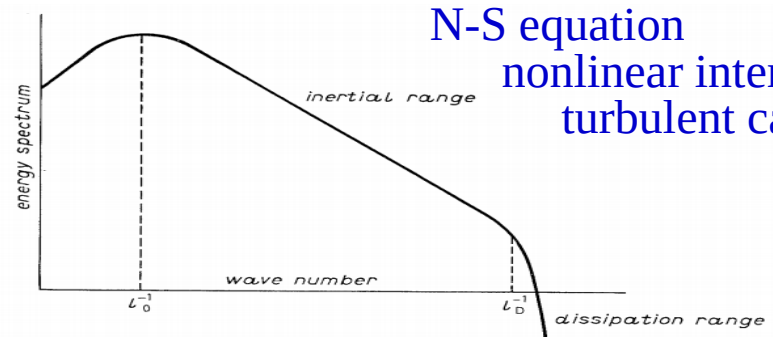

N-S equation
nonlinear interactions
turbulent cascade

Intermittency in the solar wind: PDFs as in neutral fluids

$$\delta v_\ell \sim |\mathrm{v}(r+\ell) - \mathrm{v}(r)|$$

$$\delta B_\ell \sim |\mathrm{B}(r+\ell) - \mathrm{B}(r)|$$

1. **Kappa** — Burlaga & Vinas, 2004
2. **Log-normal** — Leubner & Vörös, 2005
3. **Gaussian** — Consolini et al., 2009
4. **else?**

...instead of spatial we have temporal scales.

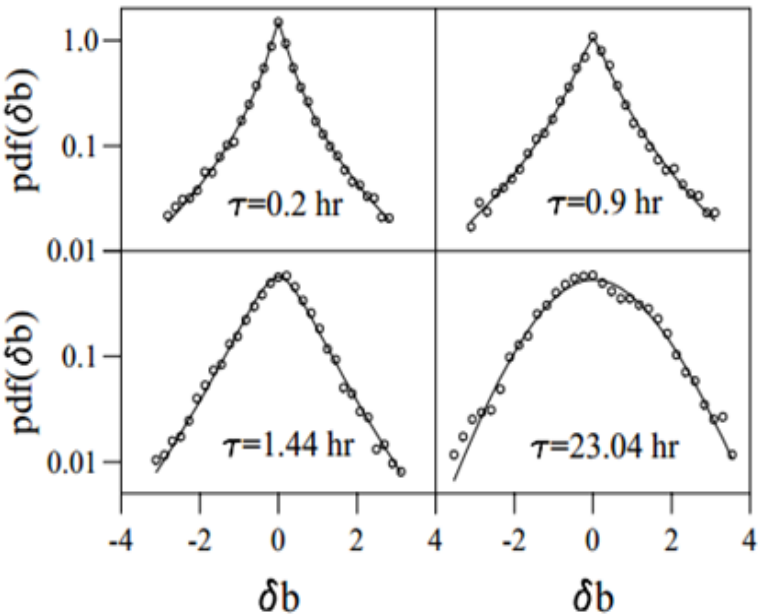

Sorriso-Valvo et al., 1999

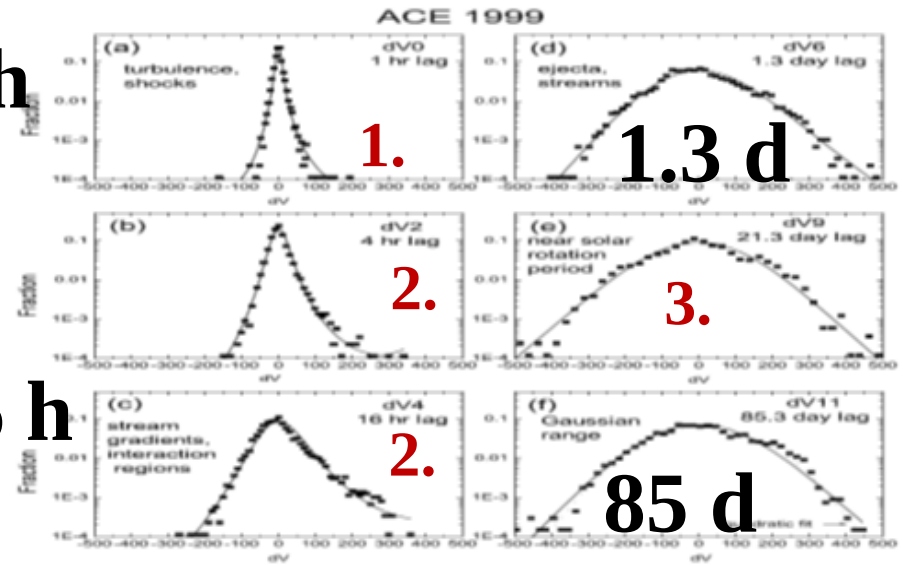

$$\mathrm{dV}\tau \equiv \mathrm{dVn}(t_i) \equiv \mathrm{V}(t_i + \tau) - \mathrm{V}(t_i)$$

Burlaga & Vinas, 2004

Correlation length: **0.015 AU- turbulence**
0.25 AU – large-scale struct.

Is there any coupling between these scales?

Kappa distribution: correlations, memory

From the Galton board:

(Leitner, Leubner & Vörös, Physica A, 2011)

$$f(v) = \frac{n}{(\pi\kappa v_\kappa^2)^{3/2}} \frac{\Gamma(\kappa+1)}{\Gamma(\kappa-1/2)} \left[1 + \frac{v^2}{\kappa v_\kappa^2}\right]^{-(\kappa+1)}$$

The normal (additive) and log-normal (multiplikative) models do not contain memory or correlations.

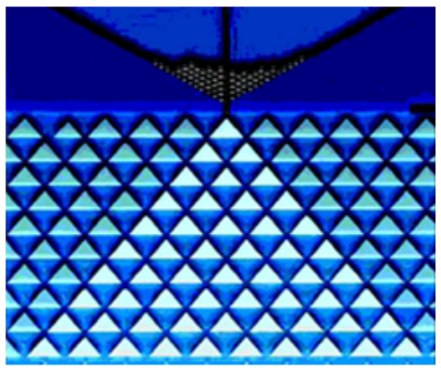

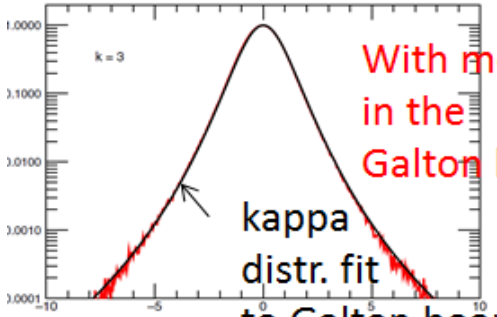

The position of a particle (ball, bean) after i rows is

$$x_i = x_{i-1} + a_1 p_i,$$

p_i is from discrete uniform distr. the ball is choosing between left or right

after N rows:

$$x_N = x_0 + a_1 \sum_{i=1}^{N} p_i$$

q_i is introduced which is a random number between -1 and 1 from a continuous uniform distribution U(-1,+1).

$$q_i = U_i(-1,\,1) + a_2 p_{i-1} |x_{i-1}| U_i(0,\,1)$$

where p_{i-1} is the result of a previous decision (± 1), $|x_{i-1}|$ or taking more previous decisions into accout:

$$q_i = U_i(-1,\,1) + \underbrace{a_2(p_{i-1} + p_{i-2} + p_{i-3} + \cdots)|x_{i-1}|U_i(0,\,1)}_{\text{MEMORY}}$$

The log-normal distribution

An example of log-normal PDF:

In biology: recursive reproduction of cells; e.g. with a mean concentration of 10^6 cells, cell division leads to double population $2*10^6$ or half population $0.5*10^6$.

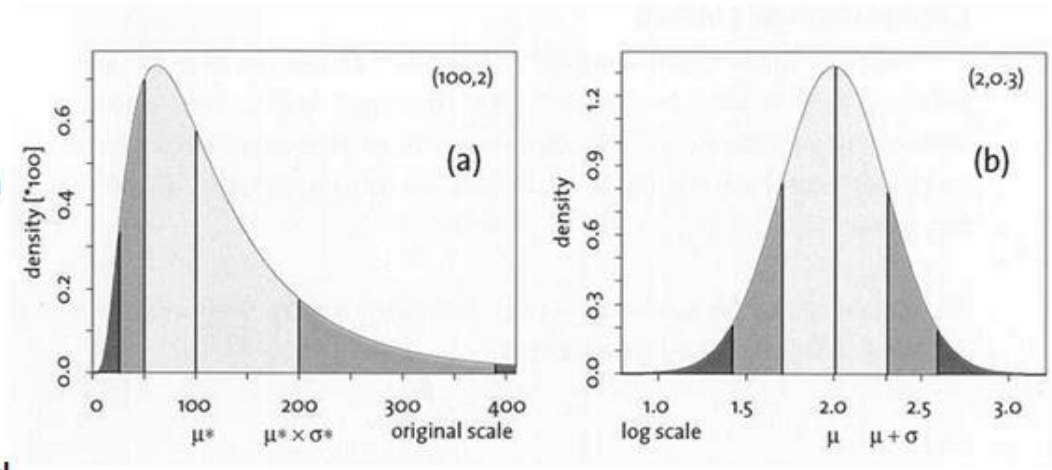

The solar wind: Compressions ‚multiply' the density or magnetic field values (Dmitriev et al. 2013).

Normal: additive

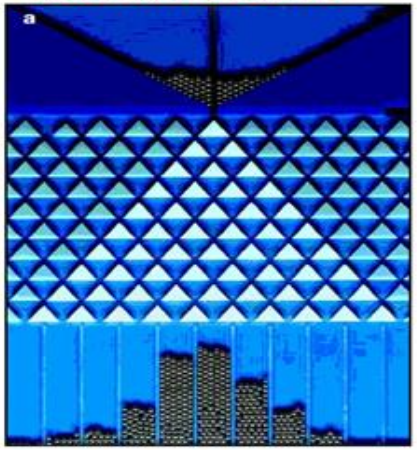

Log-normal: multiplicative

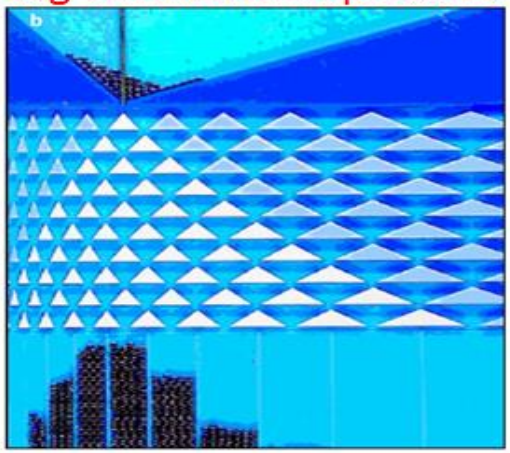

Galton board: Limpert et al., 2001

The log-kappa distribution

Correlations + multiplications = kappa + log scale

[*Leitner, Vörös & Leubner, 2009*], which is a skewed distribution like the log-normal

Multi-scale PDFs in the solar wind

Large-scale fluctuations

Large – scale fluctuations exhibit log-normal statistics within +- 2 sigma (Dmitriev et al. 2009)

OMNI database
1-h averages

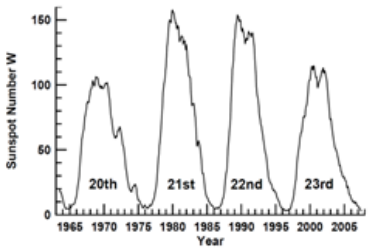

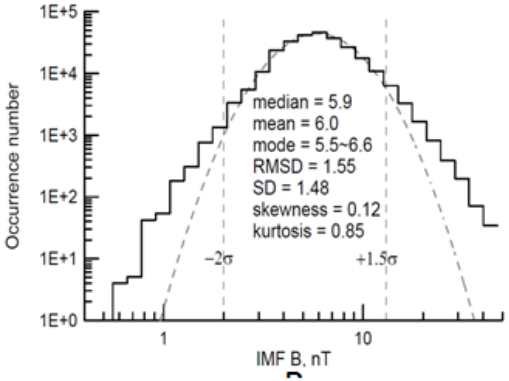

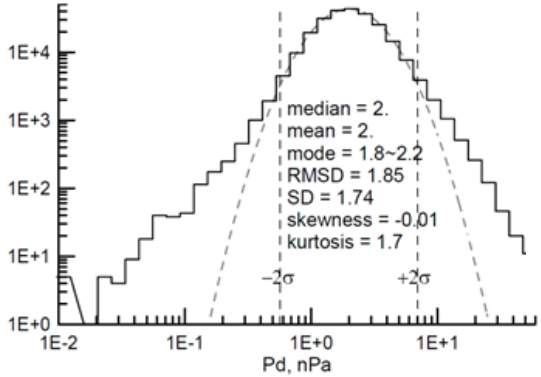

dyn.pressure

Hundhausen, 1972

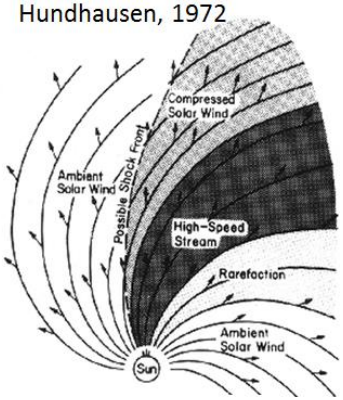

Harward-Smithonian Ctr for Astrophysics

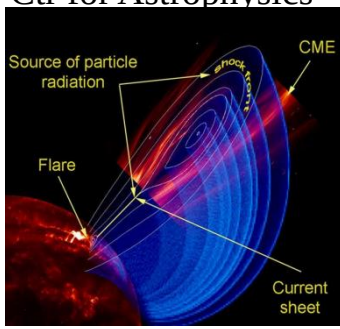

Ulysses 24 s averages

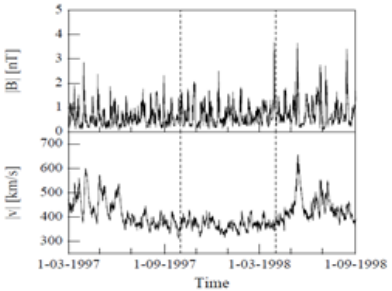

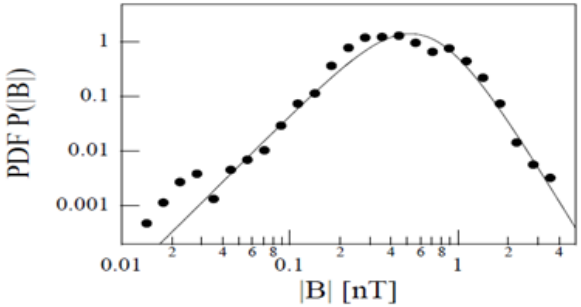

Weibul statistics (Consolini et al., 2009)

Wan et al. 2009.

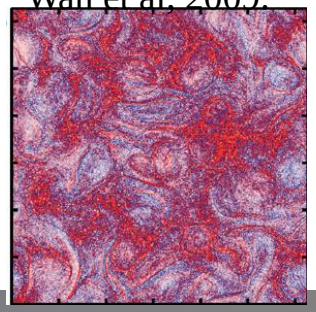

The log-normal fits indicate the occurrence of multiplicative processes in the solar wind which can be associated with compressions or amplifications of waves (Dmitriev et al., 2009; Veselovsky et al. 2010a,b.)

The PDFs are more skewed than the log-normal distribution.

Parametric PDF models for the solar wind

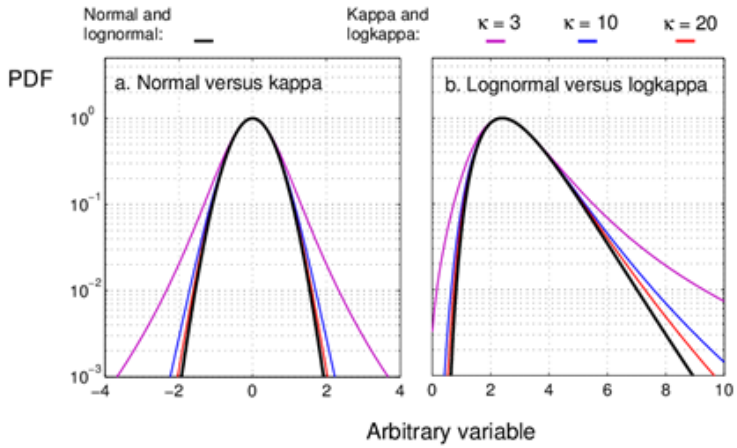

Vörös et al., 2015

Normal PDF:

$$P_n(x,\mu,\sigma) = \frac{1}{\sigma\sqrt{\pi}} \; exp\left[-\frac{(x-\mu)^2}{\sigma^2}\right]$$

Log-normal PDF:

$$P_{Ln}(x,\mu,\sigma) = \frac{1}{x} \; \frac{1}{\sigma\sqrt{\pi}} \; exp\left[-\frac{(\log x-\mu)^2}{\sigma^2}\right]$$

kappa PDF:

$$P_\kappa(x,\mu,\sigma,\kappa) = \frac{1}{\sigma\sqrt{\kappa\pi}} \; \frac{\Gamma(\kappa)}{\Gamma(\kappa-1/2)} \; \left(1+\frac{(x-\mu)^2}{\sigma^2\kappa}\right)^{-\kappa}$$

log-kappa PDF:

$$P_{L\kappa}(x,\mu,\sigma,\kappa) = \frac{1}{x} \; \frac{1}{\sigma\sqrt{\kappa\pi}} \; \frac{\Gamma(\kappa)}{\Gamma(\kappa-1/2)} \; \left(1+\frac{(\log x-\mu)^2}{\sigma^2\kappa}\right)^{-\kappa}$$

Log-kappa PDF – solar cycle minimum

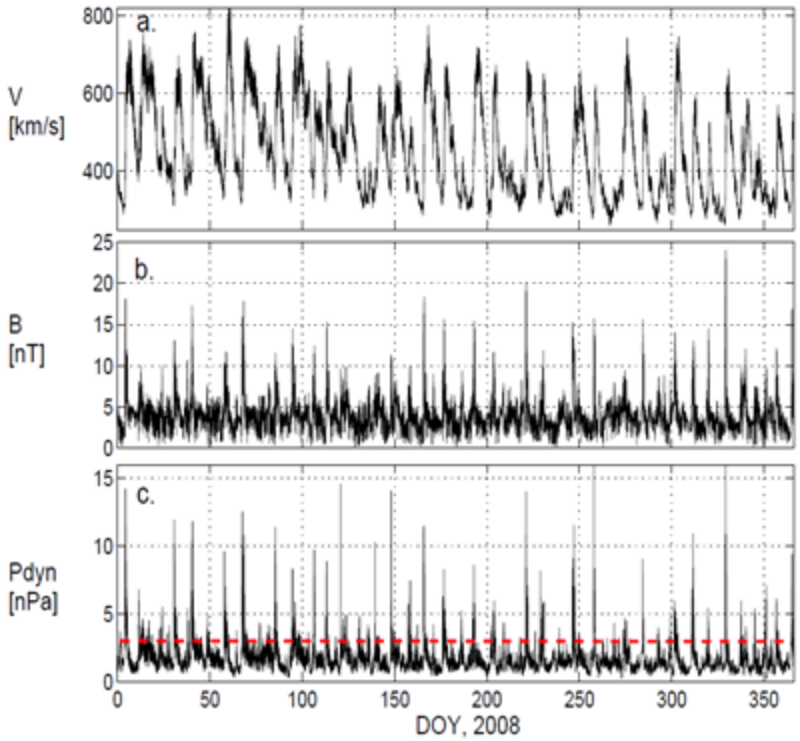

PDF(B) for the whole year 2008

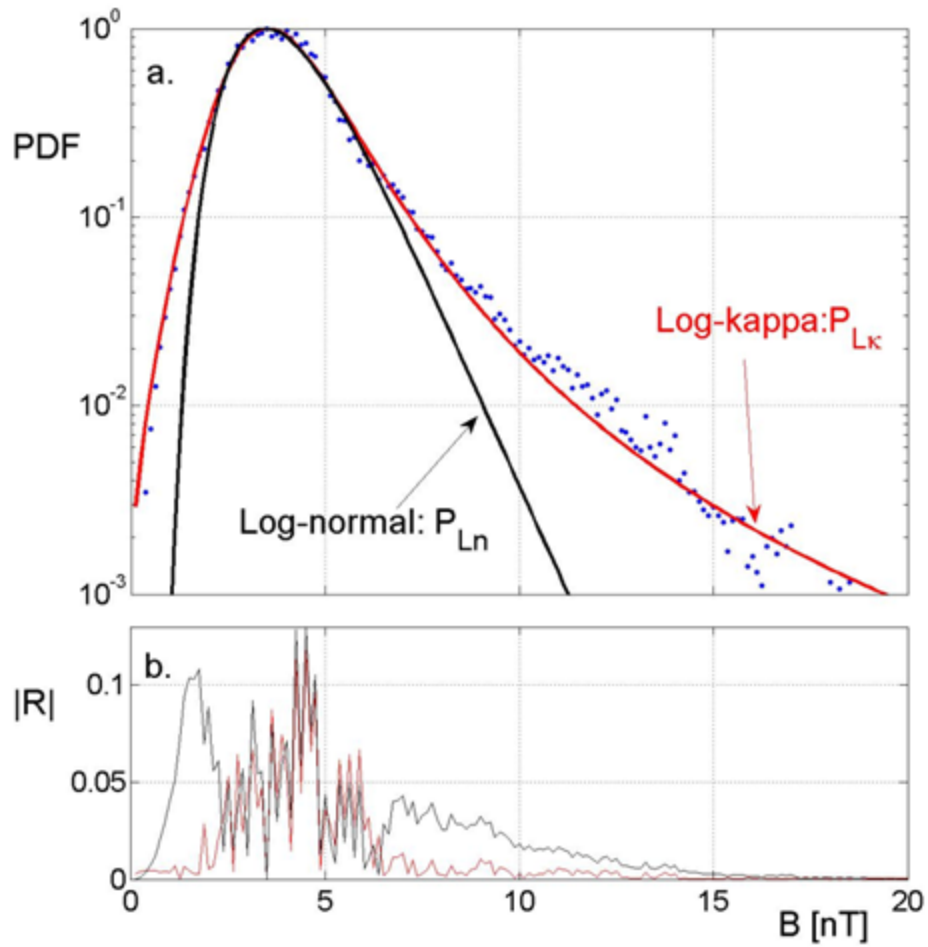

Log-normal: multiplicative, no correlations
Log-kappa: multiplicative & correlations.

Vörös et al., 2015

Conditional statistics

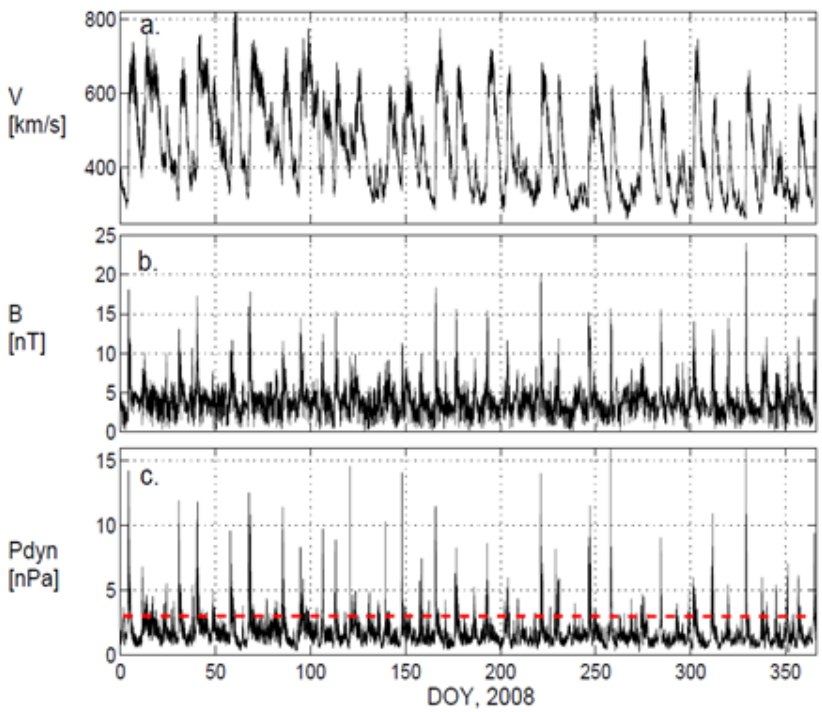

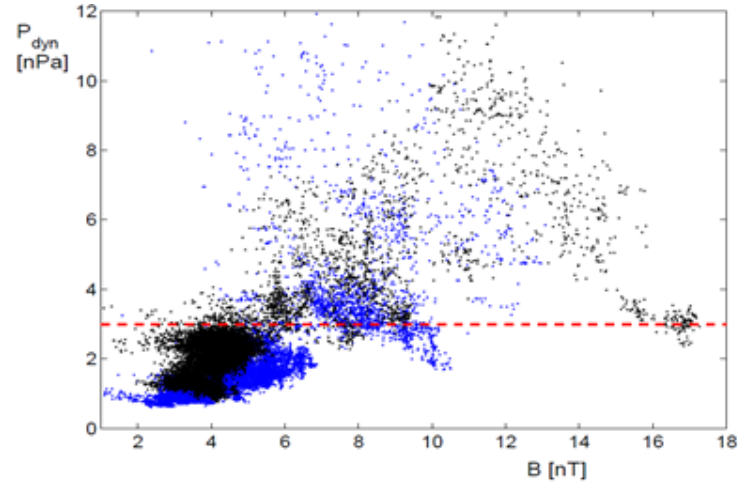

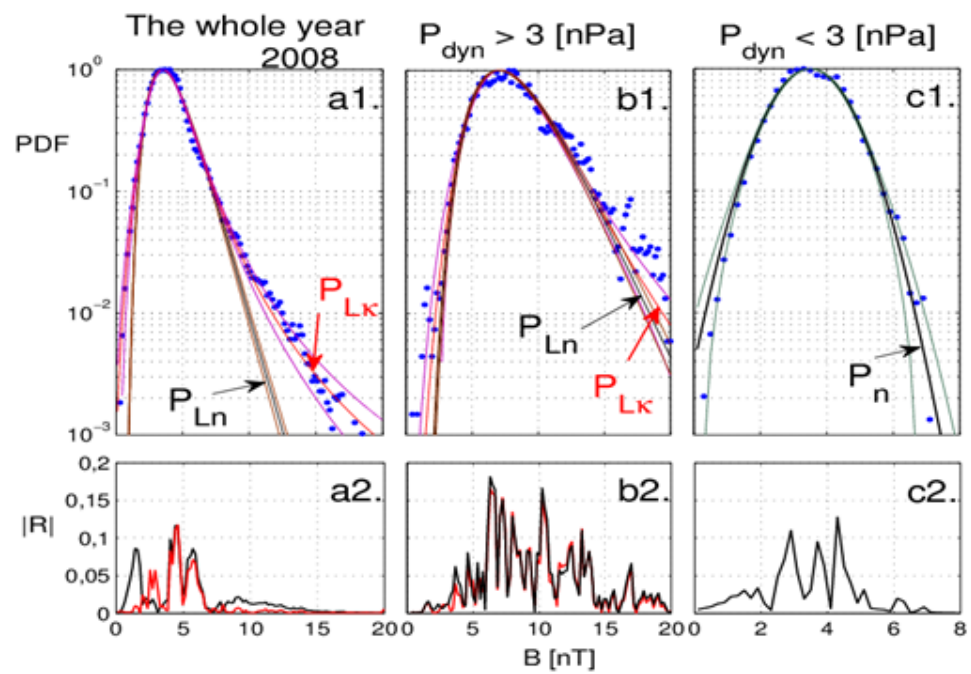

Conditional PDFs:

Uncompressional: Normal= additive

Compressional: logkappa or lognormal=multiplicative + correlations

Unconditional PDF: logkappa

= multiplicative + correlations

... and also additive

Cross-scale coupling: multi-scale vs. small-scale

Vörös et al., 2015

Time series	Skewness	PDF	μ	σ	*kappa*
B	2.4±0.1	P_{Ln}	1.36±0.01	0.49±0.01	
		$P_{L\kappa}$	1.36±0.01	0.42±0.05	3.5±0.5
B ($P_{dyn} > 3$ nPa)	2±0.1	P_{Ln}	2.06±0.01	0.46±0.01	
		$P_{L\kappa}$	2.06±0.01	0.44±0.01	8±4
B ($P_{dyn} < 3$ nPa)	0.1±0.1	P_n	3.5±0.01	2±0.15	

Table 1. PDF model fitting statistics for the multi-scale magnetic fluctuations (B). σ, μ are in [nT] for the P_n model.

Time series	Skewness	PDF	μ	σ	*kappa*
δB	0.15±0.1	P_n	0	0.032±0.01	
		P_κ	0	0.03±0.01	1.2±0.05
δB ($P_{dyn} > 3$ nPa)	0.1±0.1	P_n	0	0.2±0.05	
		P_κ	0	0.18±0.05	1.1±0.2
δB ($P_{dyn} < 3$ nPa)	0±0.05	P_n	0	0.04±0.002	
	0±0.05	P_κ	0	0.039±0.002	1.58±0.05

Table 2. PDF model fitting statistics for the time-delayed magnetic fluctuations (δB). σ, μ are in [nT] for the P_n and the P_κ models.

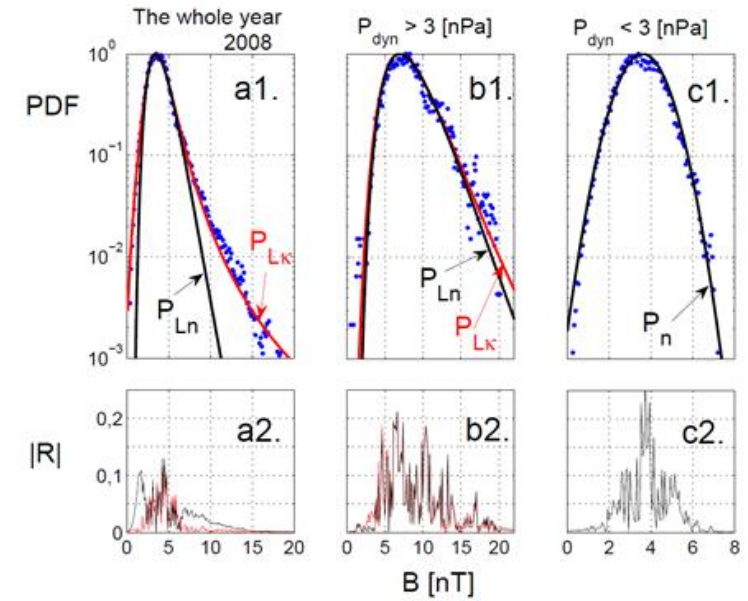

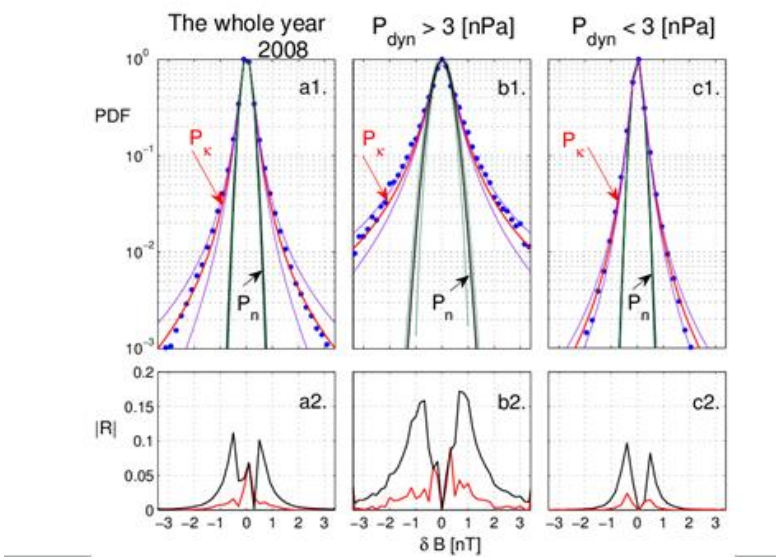

Conclusions I.

- Conditional statistics is necessary for understanding of multi-scale multi-component processes

- Large-scale structures modify turbulent statistics over the small-scales

- Solar wind fluctations: mixture of additive, multiplicative processes exhibiting correlations

In the limit of large kappa

- kappa = normal
- log-kappa = log-normal

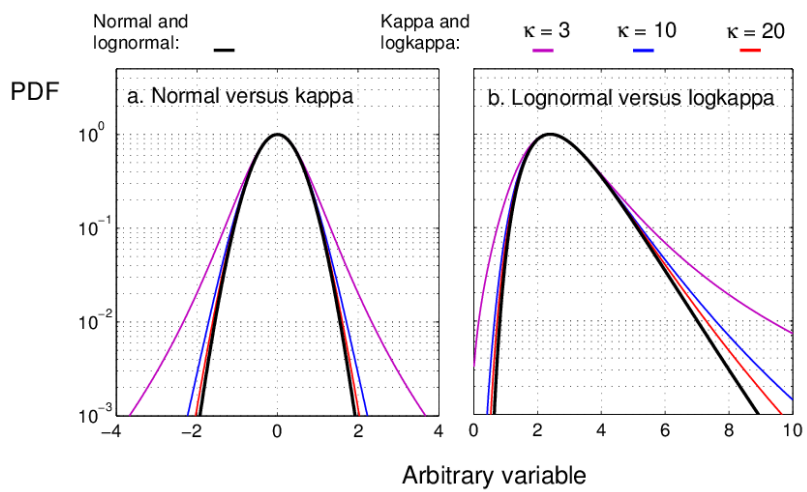

Intermittency and structure formation

Intermittency in the solar wind: challenges

$$\mathbf{Z}^{\pm}(t) = \mathbf{v}(t) \pm \mathbf{b}(t)/\sqrt{4\pi\rho}$$ Elsässer variables

$$\frac{\partial \mathbf{Z}^{\pm}}{\partial t} + (\mathbf{Z}^{\mp} \cdot \nabla)\mathbf{Z}^{\pm} = -\nabla P + \eta' \nabla^2 \mathbf{Z}^{\pm}$$

The nonlinear term is responsible for the local transfer of energy between adjacent scales.
However, additional correlations can compete or supress the nonlinear term (Matthaeus et al, 2015).

Alfvénic with $v \propto b$, reduces $\frac{\partial \mathbf{B}}{\partial t} = \nabla \times (\mathbf{V} \times \mathbf{B}) + \eta \nabla^2 \mathbf{B}$ induction equation

force free with $b \propto \nabla \times b$, $\rho \frac{\partial \mathbf{v}}{\partial t} + \rho(\mathbf{v} \cdot \nabla)\mathbf{v} = -\nabla p + \mathbf{j} \times \mathbf{B}$

the Lorentz force $= \frac{1}{\mu}(\nabla \times \mathbf{B}) \times \mathbf{B}$

Beltrami with $v \propto \nabla \times v$. $v \times (\nabla \times v)$

2D ideal compressible MHD

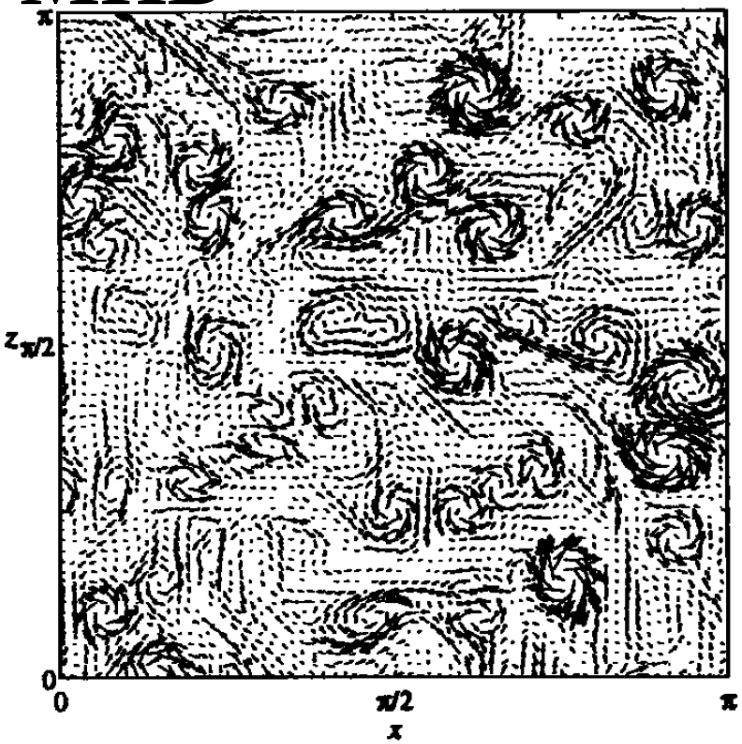

Magn. field
Wu & Chang, 2000

Ideal **Resistive MHD**

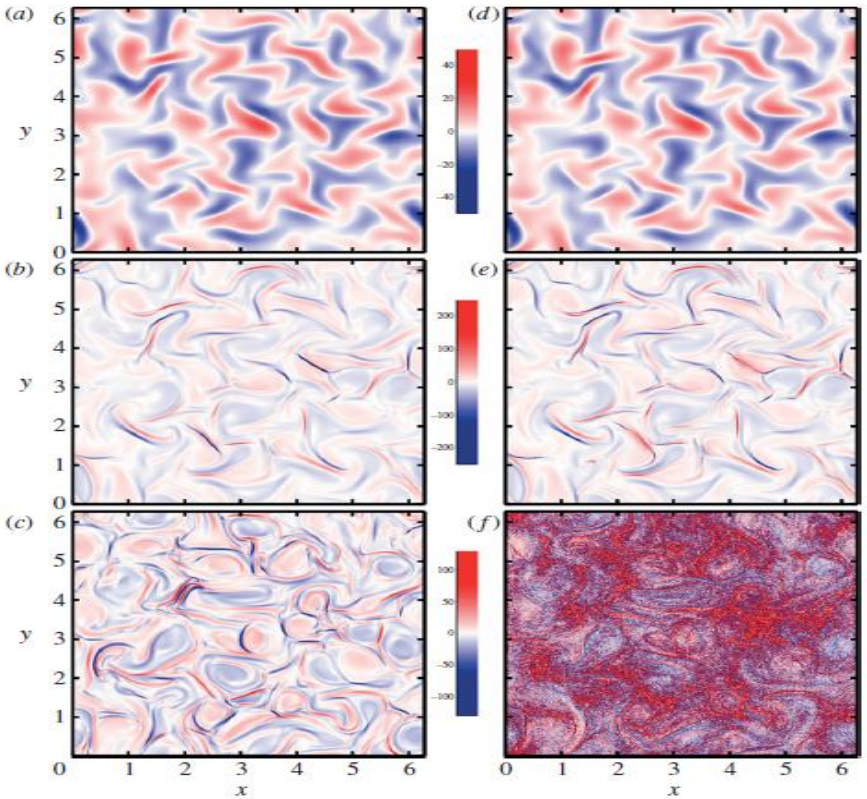

Current density: sheet-like structures; **Wan et al., 2009**; Coherent structures of non-dissipative origin

Simulation results: turbulence and structures

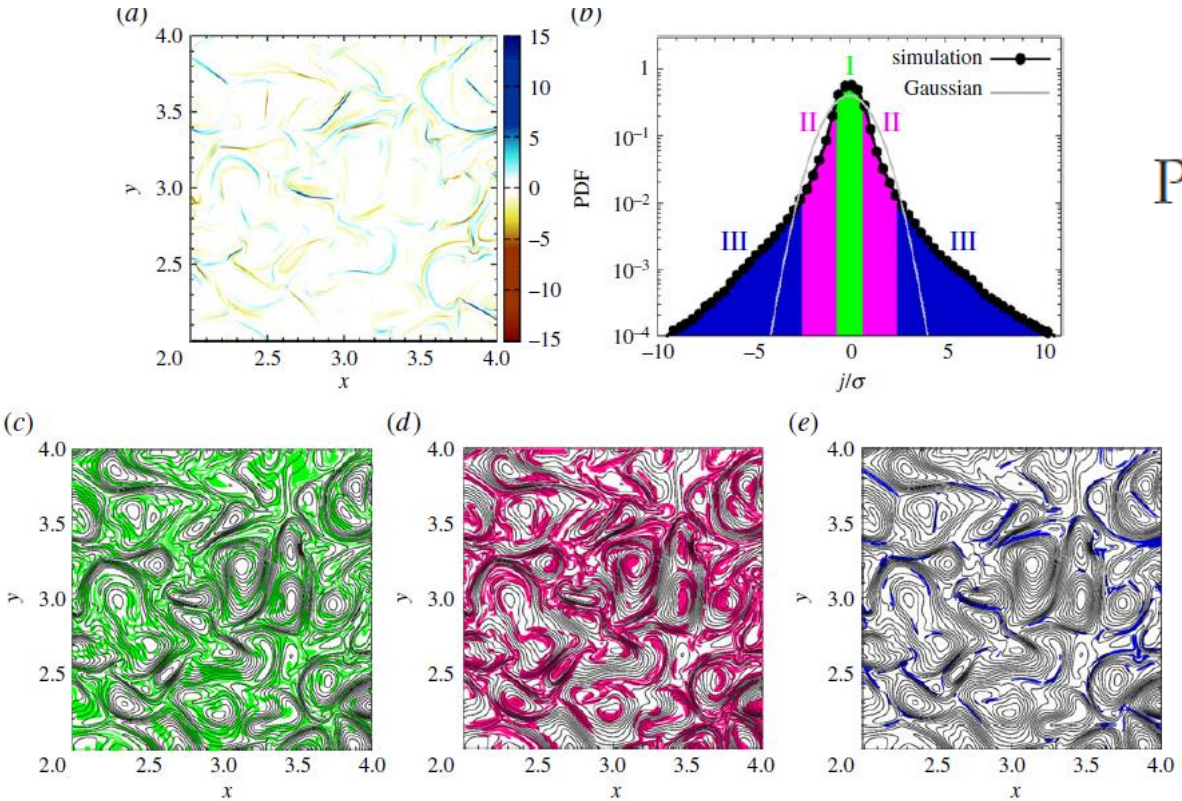

Matthaeus et al., 2015

$$\mathrm{PVI}(s;\tau) = \frac{|\Delta B(s,\tau)|}{\sqrt{\langle |\Delta B(s,\tau)|^2 \rangle}}$$

The partial variance of increments (PVI)

$$\Delta B(s,\tau) = B(s+\tau) - B(s)$$

allows to detect the current sheets or discontinuities, or flux tube walls (Greco et al., 2008), at which heating occurs (Osman et al. 2011).

2D MHD, moderate Re
electric current density + B

Conclusions II.

- Simulations indicate that turbulence can generate structures, current sheets, discontinuities, which can be flux rope walls,

- The structures are associated with the long tails of the PDFs,

- The structures in both simulations and experiments are places of reconnection and heating,

Although turbulence can generate coherent structures in the solar wind, there is a large variety of structures which are not generated by turbulence.

Reconnection generated turbulence

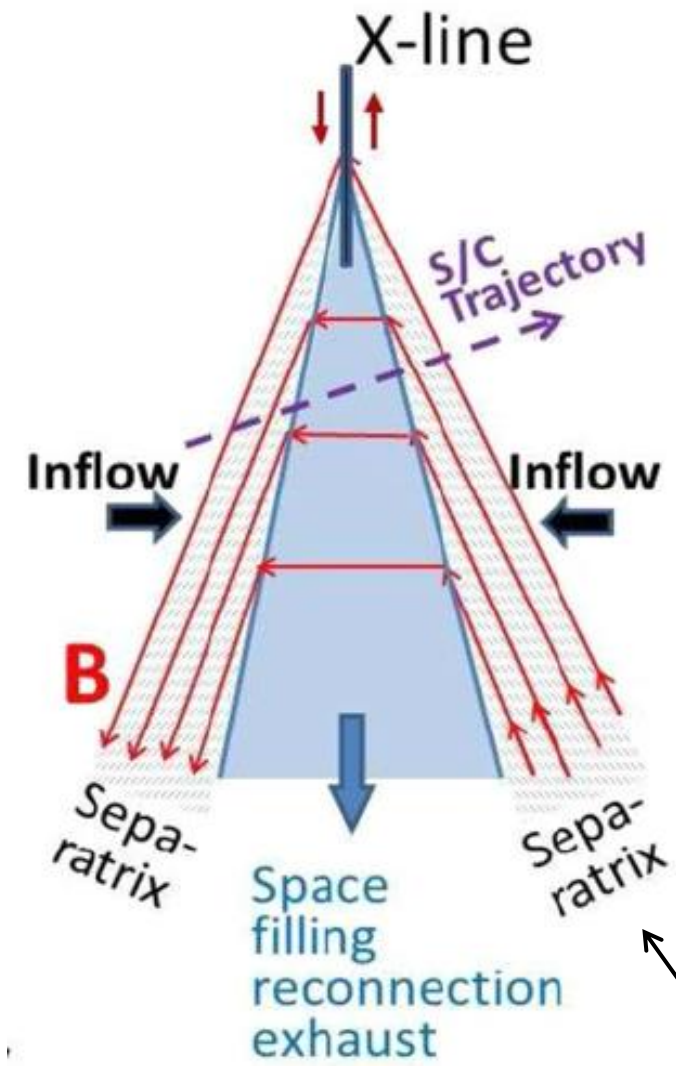

Vörös et al., 2014

The newly reconnected field lines associated with plasma inflow through the separatrix are kinked.

The kinks representing a pair of Alfvenic discontinuitie or RDs in the inflow regions are accelerating plasmas to the exhaust.

Usually the exhausts contain plasmas with decreased B and enhanced Tp and Np, the transition to the exhaust is a slow-mode shock. (Gosling, 2013).

Enhanced fluctuations near the exhaust boundaries (Huttunen et al., 2007).

Reconnection generated turbulence

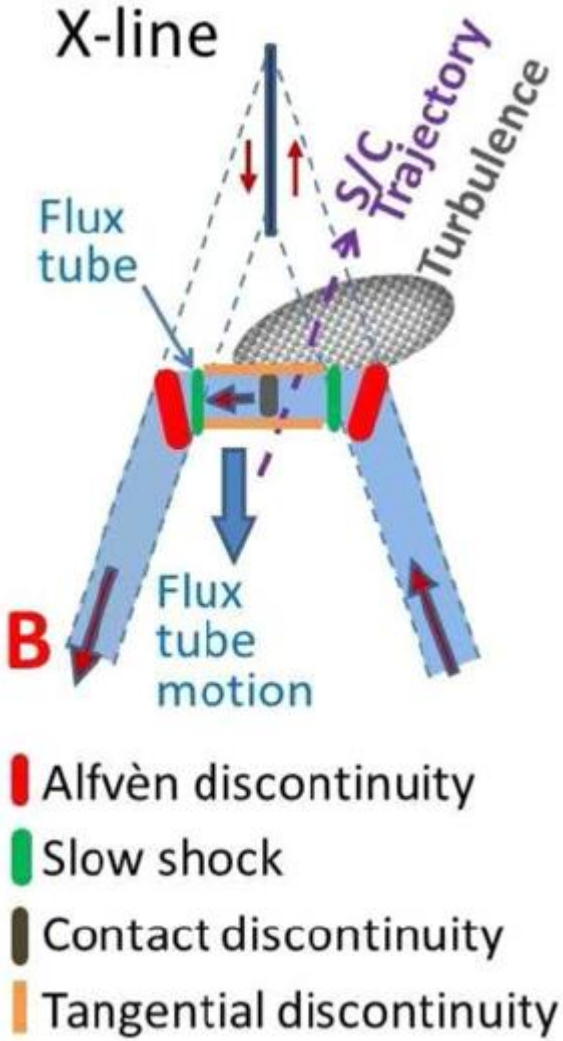

Vörös et al., 2014

An unstable current sheet, via reconnection, decays into a system of moving large amplitude fast, slow, Alfven waves.

The waves propagate along the current sheet together with the reconnected plasma and magnetic flux, collectively forming the outflow region with embedded discontinuities and a propagating flux tube. (Sasunov et al. 2012).

The flux tube can be K-H unstable TD generating turbulence and heating.

Example: reconnection outflow

Vörös et al. 2014

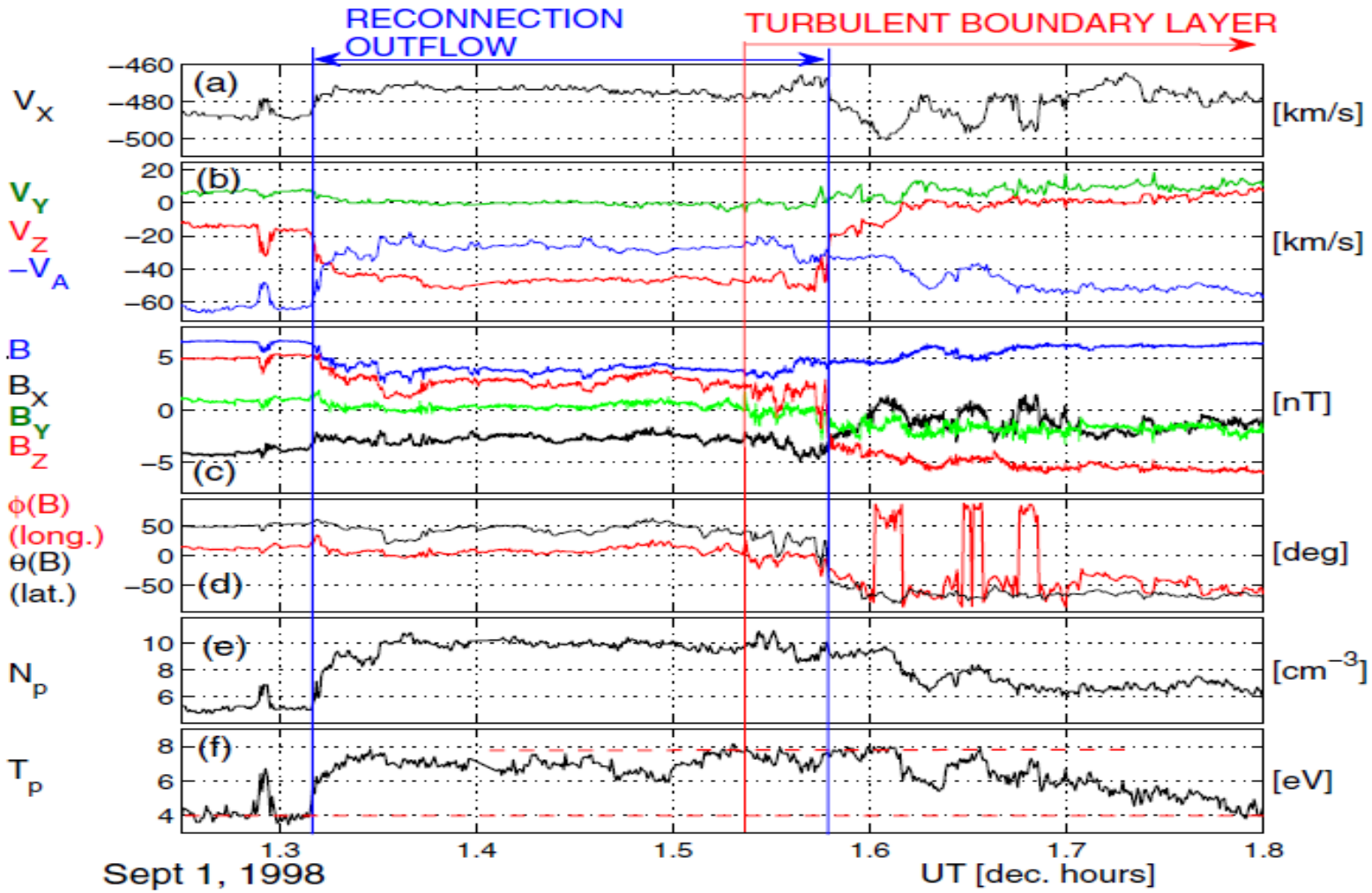

Reconnection outflow: spectral features

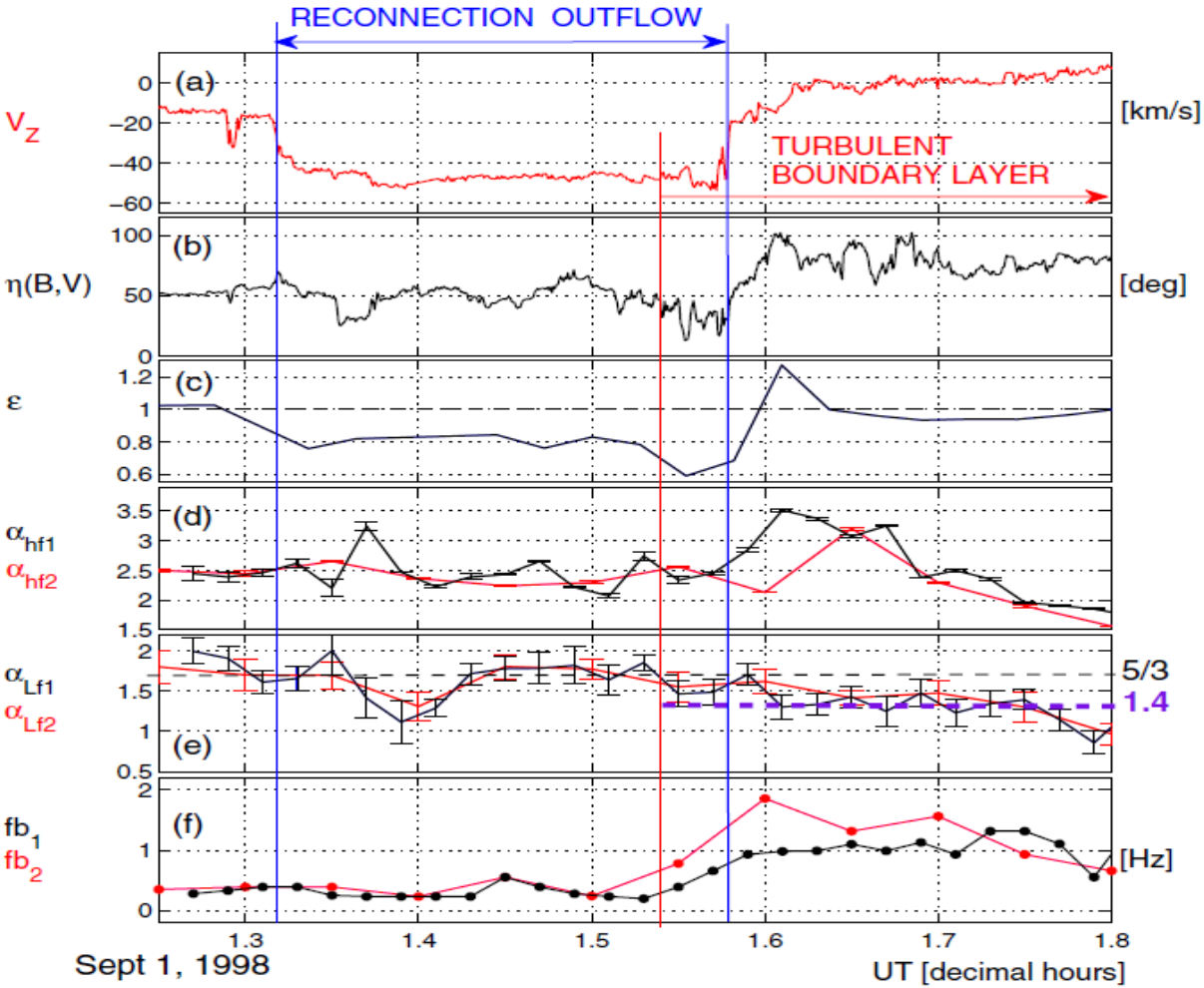

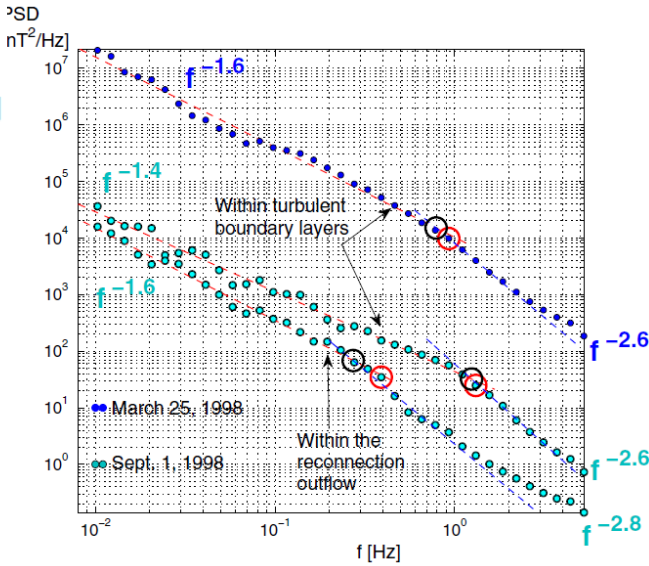

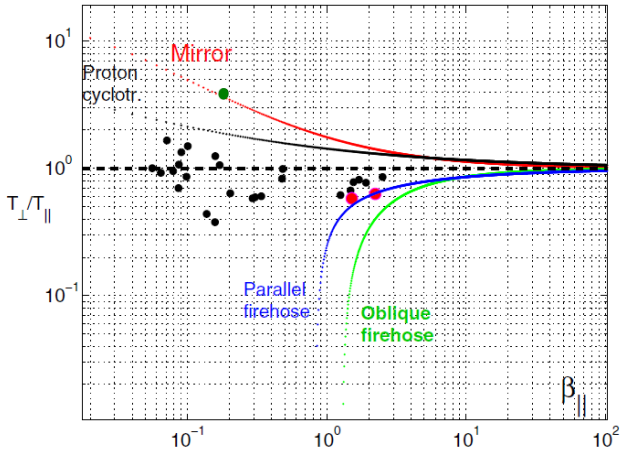

Vörös et al. 2014

$$\epsilon = 1 - \mu_0(P_{||} - P_\perp)/B^2$$

$\eta(\langle \mathbf{B} \rangle, \mathbf{V}) < 30^\circ$ field-aligned fluctuations

Conclusions III.

- In both reconnection scenarios turbulence can be generated locally,

- The turbulent layer contains a slowly cooling-mixing plasma exhibiting a fluctuating temperature-density profile with embedded directional changes of B,

- In the reconnection database of Phan et al., (2009) we found that 27 outflow events (out of 51) were accompanied by a turbulent boundary layer.

Magnetic flux tubes

Laboratory, space and astrophysical plasmas self-organize themselves to non-space-filling coherent structures (Alfven 1951).

Flux tubes are volumes enclosed by magnetic field lines which intersect closed curves (Priest, 1991, 2014).

Laboratory
(electron cyclotron emission imaging)

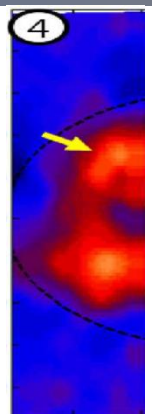

Tokamak
Yun et al., 2012

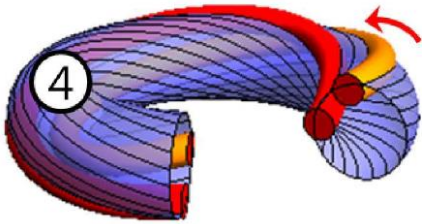

Cheng et al., 2014

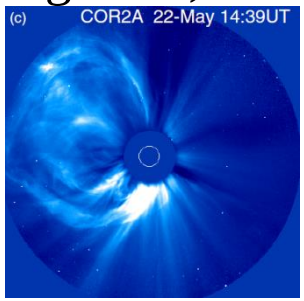

Space
(**remote** observation of a coherent structure within a white-light CME)

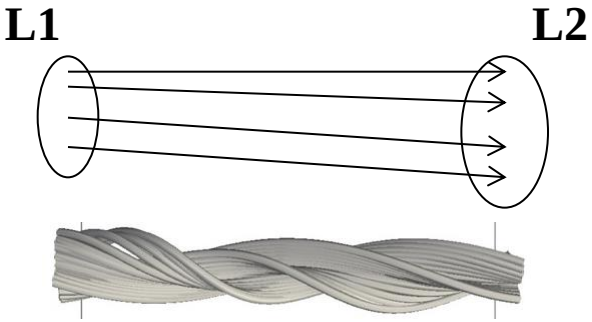

Markidis et al., 2014

Space
(**in-situ** observations: trajectories of the tips of **B** in the solar wind)

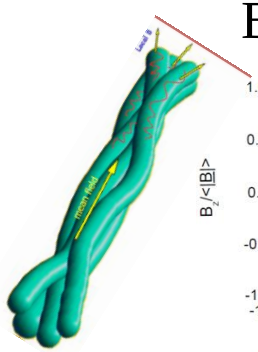

Bruno et al., 2001

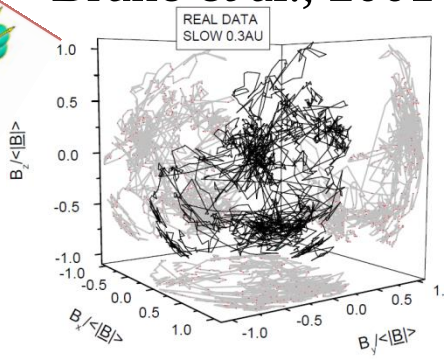

Magnetic flux tubes

Laboratory, space and astrophysical plasmas self-organize themselves to non-space-filling coherent structures (Alfven 1951).

Flux tubes are volumes enclosed by magnetic field lines which intersect closed curves (Priest, 1991, 2014).

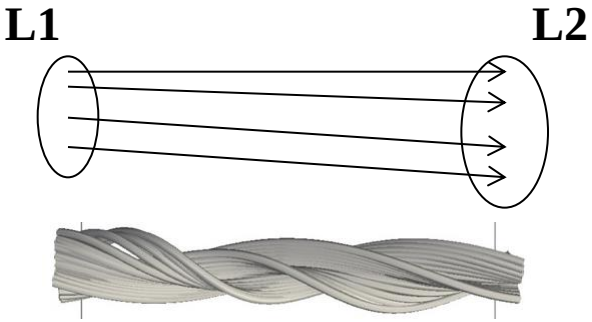

Markidis et al., 2014

Space
(**in-situ** observations: Flux transfer events at the magnetopause)

Russel & Elphic, 1978,1979

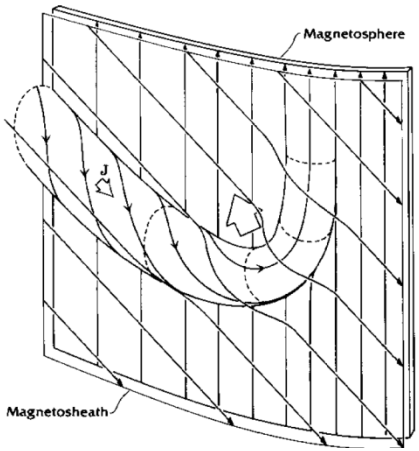

Space
(**in-situ** observations: Transport of flux ropes from the dayside to the flank tail)

Eastwood et al., 2014

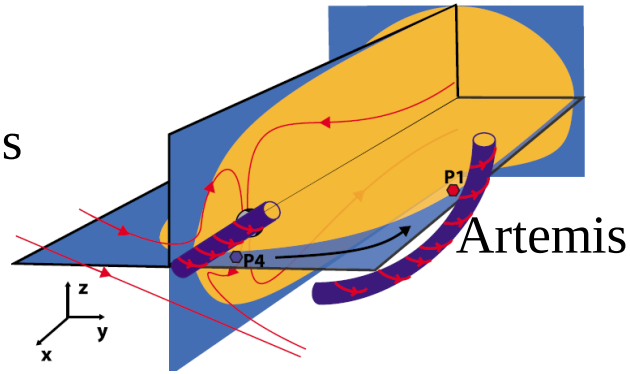

Artemis

Themis

Magnetic flux tubes

Laboratory, space and astrophysical plasmas self-organize themselves to non-space-filling coherent structures (Alfven 1951).

Flux tubes are volumes enclosed by magnetic field lines which intersect closed curves (Priest, 1991, 2014).

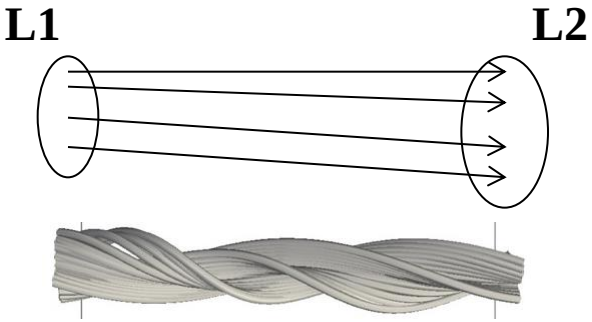

Markidis et al., 2014

Space

(**in-situ** observations: Flux tubes/plasmoids in the Earth's magnetotail)

Hietala et al., 2014

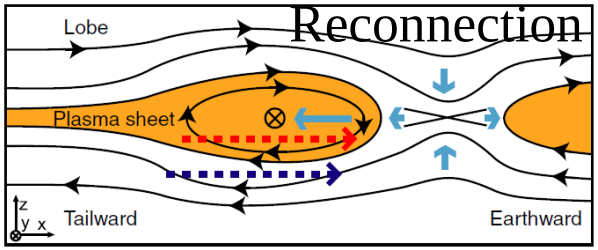

Vörös et al., 2014

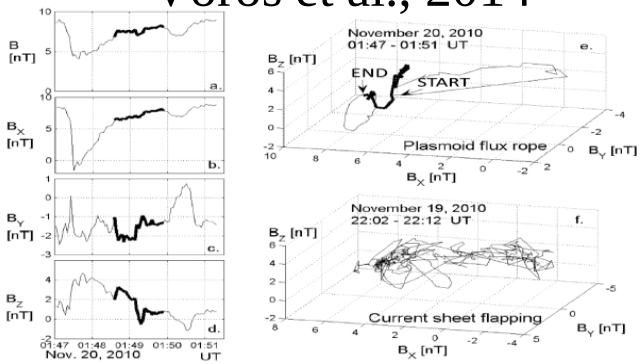

Astrophysics

(**remote** observation: Double helix nebula)

Morris et al., 2006
Spitzer Space Telescope

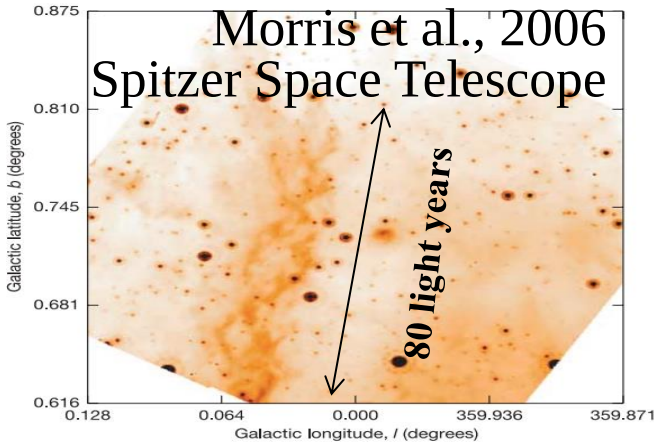

Twisted magnetic flux tubes

Multi-wavelength observations:

magnetic flux can be transported from the solar interior into the atmosphere and corona in the form of TWISTED flux tubes (Okamoto et al. 2008; Srivastava et al., 2010).

Simulations:

The bodily emergence of coherent flux tubes requires a nonzero TWIST (Hood et al. 2009).

Observations:

A CME is the eruption of a coherent magnetic, TWIST carrying coronal structure... (Vourlidas et al., 2013)

Image Credit: NASA/Goddard Space Flight Center

Loop with helical twist

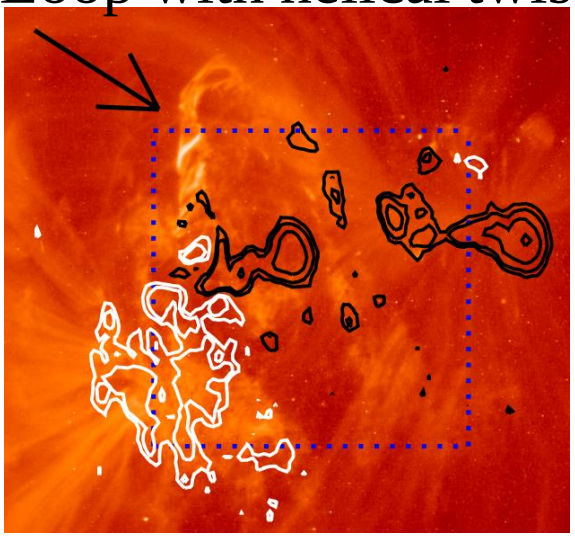

ACTIVE REGION

SOHO/MDI contours on TRACE 171 A image on June4, 2007. White/black contours show positive/negative polarity. **Srivastava et al. 2010.**

Twisted tubes in the solar wind

Observations:

Lynch et al.,2005;
Feng et al. 2007,2008;
Lepping and Wu, 2010;
Cartwright and Moldwin, 2010;
Janvier et al., 2014

DURATION:
0.5 - 40 hrs
ORIGIN:
Sun, HCS, MR,?

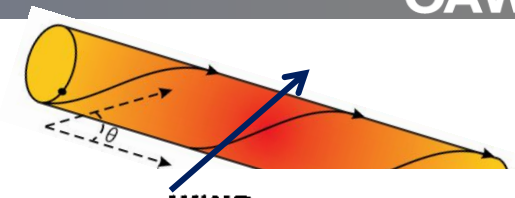

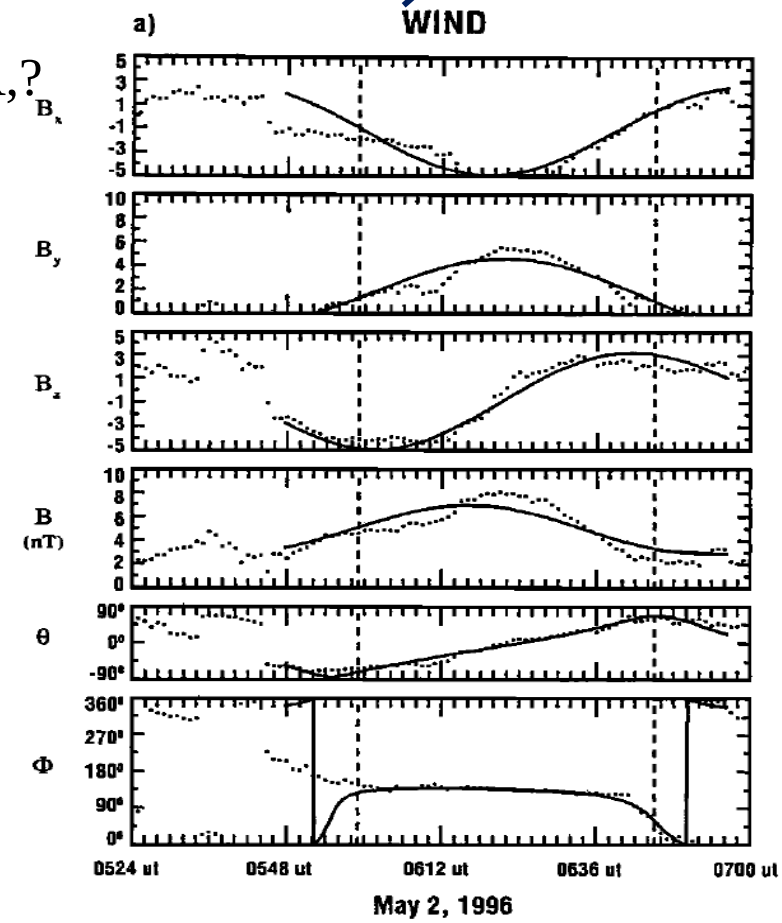

Moldwin et al., 2000

Model:

Force free: plasma β << 0.5

$$\rho \frac{d\mathbf{v}}{dt} = -\nabla p + \mathbf{j}\times\mathbf{B} \qquad \nabla \times \mathbf{B} = \mu_0 \mathbf{J} + \mu_0 \varepsilon_0 \frac{\partial \mathbf{E}}{\partial t}$$

$$(\nabla \times \mathbf{B}) \times \mathbf{B} = \mathbf{0} \quad \Longrightarrow \quad \nabla \times \mathbf{B} = \alpha\, \mathbf{B}$$

$$\nabla \times (\nabla \times \mathbf{B}) = \alpha(\nabla \times \mathbf{B}) = \alpha^2 \mathbf{B}$$

Force free solution (Lundquist, 1950) in cylindrical coordinates:

$$(0, B_\theta(r), B_z(r)) \qquad B_z = B_0 J_0(\alpha r), \qquad B_\theta = B_0 J_1(\alpha r)$$

Twisted tubes in the solar wind

The force-free model $\mathbf{j}\times\mathbf{B}=\mathbf{0}$ has limitations regarding the real magnetic field structure mainly for small-scale twisted tubes for which $\beta > 0.5$.

We propose a model for the twisted magnetic tubes based on the observations of the total (thermal+magnetic) pressure. This removes the limitations of the force-free approach.

In $(0, B_\phi(r), B_z(r))$ $\quad \mathbf{0} = -\nabla p + \mathbf{j}\times\mathbf{B} \longrightarrow \dfrac{dP_{T0}}{dr} = -\dfrac{B_\phi^2}{4\pi r},$ **Pressure balance condition inside the tube**

$$P_{T0} = P_0 + \frac{B_z^2 + B_\phi^2}{8\pi}$$ **Total pressure**

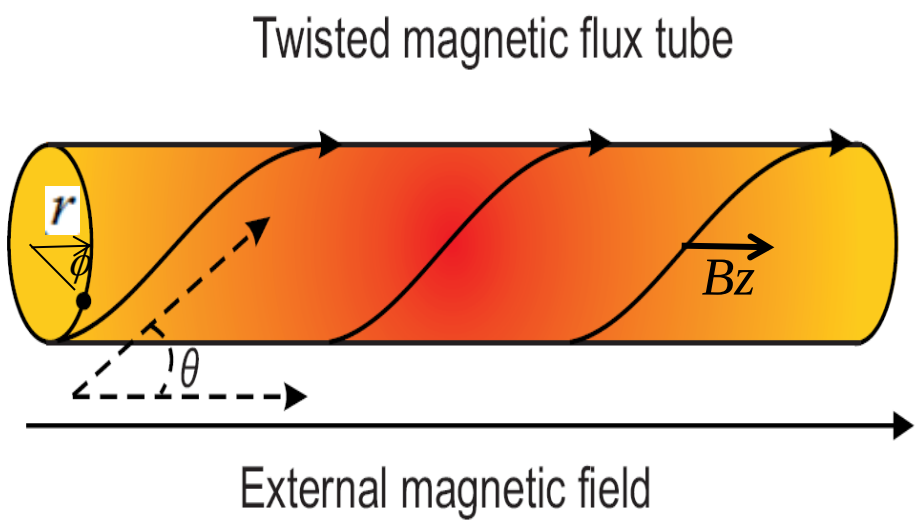

$$P_{T0}(r) = P_{T0}(0) - \frac{1}{4\pi}\int_0^r \frac{B_\phi^2(s)}{s}ds.$$

The total pressure is not constant across the tube and its structure depends on twist!

Wind observations of twisted tube

WIND observation of a twisted magnetic tube. The same event was analyzed by Feng et al. (2007) and Telloni et al. (2012) .

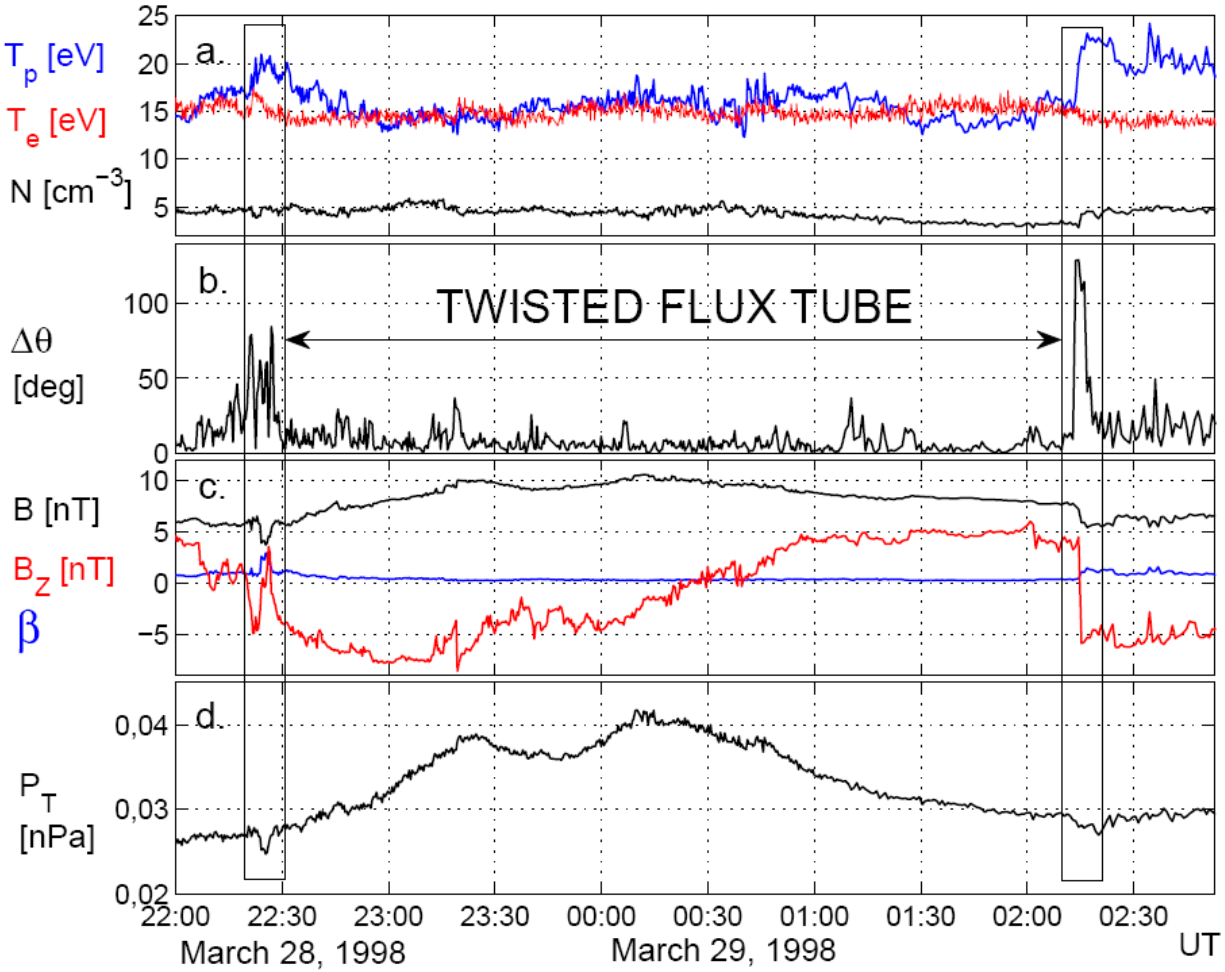

Zaqarashvili, Vörös, Narita and Bruno, ApJL 2014

Total pressure profile

Red solid line: theoretical profile of total pressure in the tubes with $B_\phi(r) = Ar$
Black line: Feng et al. (2007)
Green, magenta, blue and purple lines: Moldwin et al. (2000)

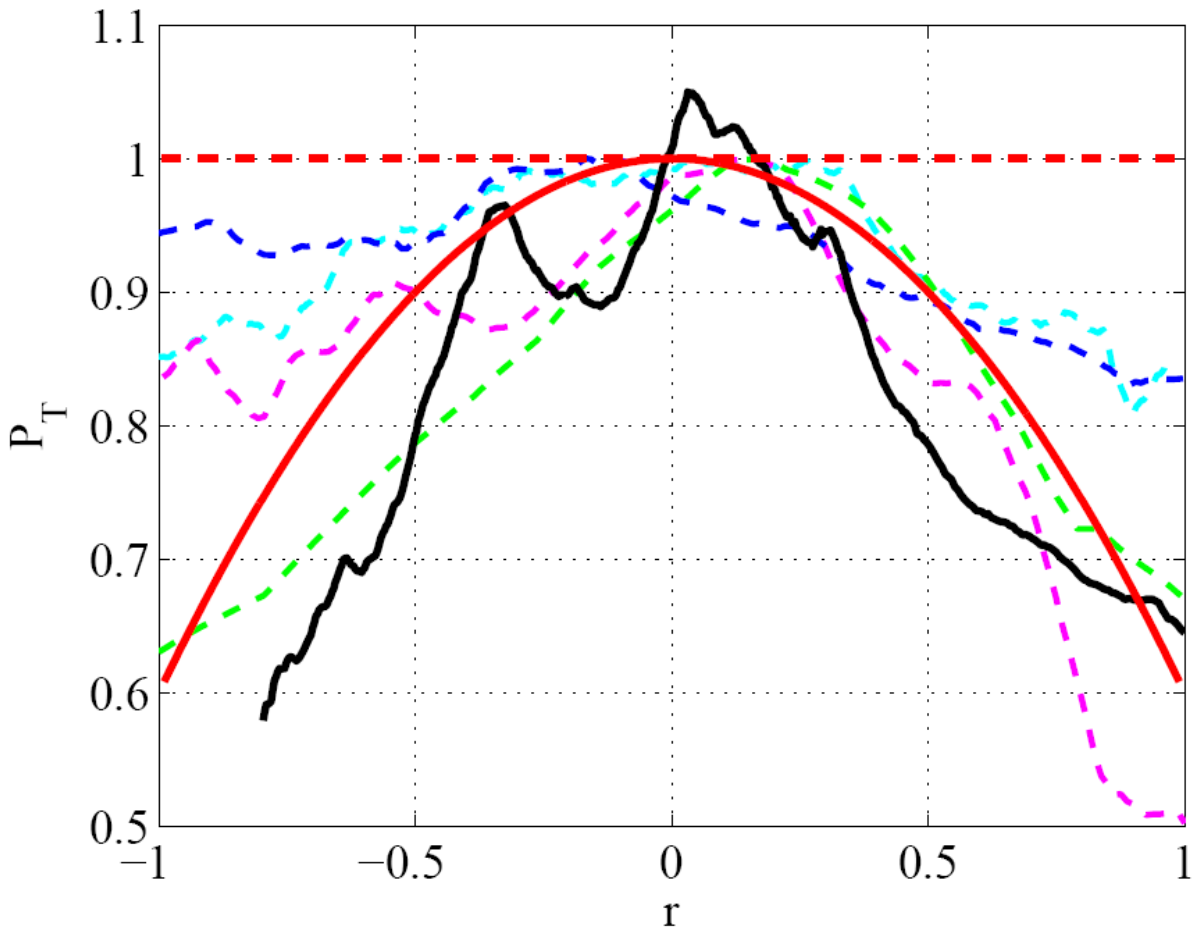

Zaqarashvili, Vörös, Narita and Bruno, ApJL 2014

Kink instability of twisted tubes

The twisted tubes are subjects to the kink instability when the twist exceeds a critical threshold value.

The instability may trigger the magnetic reconnection near boundary owing to kinking motion, which may lead to remove the additional twist from the tube.

Therefore, it is interesting to find the critical twist angle for solar wind tubes.

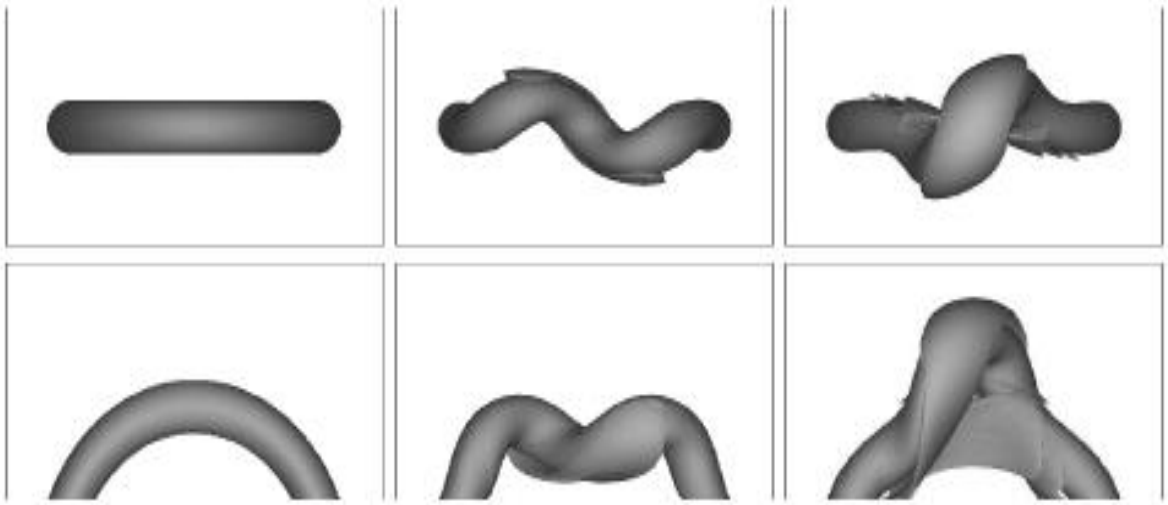

Török and Kliem 2004

An external magn.field can increase the threshold and stabilize the instability (Benett et al. 1999). However, a flow along the tube may decrease the critical threshold (Zaqarashvili et al., 2010)

Solutions inside and outside the tube

Inside the tube:
constant density ρ_0 , $(0, Ar, B_z)$.

Outside the tube:
constant density ρ_e, $(0,0,B_{ze})$

The magnetic tube is moving along Z by speed –U. To obtain the dispersion relation governing the dynamics of the tube, the linearized MHD equations are perturbed by $\exp[i(m\phi + kz - \omega t)]$ and Bessel equations for total pressure are obtained inside and outside of the tube (Dungey and Loughhead, 1954)

$$\frac{d^2 p_t}{dr^2} + \frac{1}{r}\frac{dp_t}{dr} - \left(\frac{m^2}{r^2} + m_0^2\right) p_t = 0,$$

where k is the longitudinal wavenumber, ω is the frequency

$$m_0^2 = k^2\left(1 - \frac{4A^2\omega_A^2}{4\pi\rho_0(\omega^2 - \omega_A^2)}\right), \qquad \omega_A^2 = \frac{mA + kB_z}{\sqrt{4\pi\rho_0}}.$$

The bounded solution at the tube axis is

$$p_t = a_0 I_m(m_0 r).$$

The bounded solution at infinity is

$$p_t = a_e K_m(kr).$$

Dispersion equation

Continuity of Langrangian displacement and Lagrangian pressure at the tube surface leads to the transcendental dispersion equation

$$\frac{\sqrt{4\pi\rho_0}\left(\omega^2-\omega_A^2\right)F_m(m_0a)-2m\omega_A}{\sqrt{4\pi\rho_0}\left(\omega^2-\omega_A^2\right)^2-4\omega_A^2A^2}=\frac{\sqrt{4\pi\rho_0}P_m(ka)}{\sqrt{4\pi\rho_0}\left(\left(\omega-kU\right)^2-\omega_{Ae}^2\right)\left(\rho_e/\rho_0\right)+P_m(ka)},$$

where

$$F_m\left(m_0a\right)=\frac{m_0aI_m^{'}\left(m_0a\right)}{I_m\left(m_0a\right)};P_m\left(m_0a\right)=\frac{kaK_m^{'}\left(ka\right)}{K_m\left(ka\right)}.$$

Marginal stability analysis in the thin tube approximation gives the criterion for the kink (m=1) instability as

$$B_\phi(a)>2B_z\left(1+\frac{kB_z}{A}\right)\sqrt{1-\frac{\rho_e}{\rho_0}M_A^2+\mu^2},$$

where $\mu=\dfrac{B_e}{B_z}$ and $M_A=\dfrac{U}{V_{A0}}$ is the Alfvén Mach number.

Critical twist angle

The critical twist angle for the kink instability can be approximated as

$$\theta_c = \arctan\left(\frac{B_\phi(a)}{B_z}\right) \approx \arctan\left(2\sqrt{1-\frac{\rho_e}{\rho_0}M_A^2+\mu^2}\right).$$

The critical twist angle decreases when μ decreases and M_A increases.
Maximum critical twist angle (~70^0) occurs for μ=1 and M_A=0.
The tubes twisted with >70^0 angle are always unstable for the kink instability.

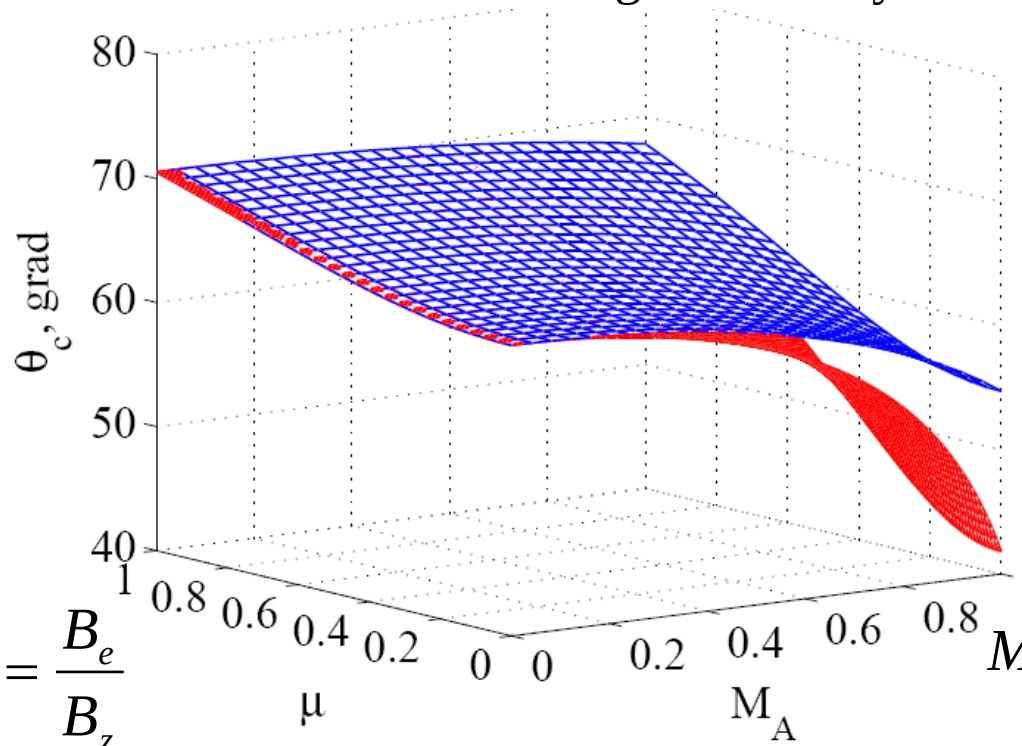

Red surface: $\frac{\rho_e}{\rho_0} = 0.8$

Blue surface - $\frac{\rho_e}{\rho_0} = 0.5$

$$\mu = \frac{B_e}{B_z} \qquad M_A = \frac{U}{V_{A0}}$$

Zaqarashvili, Vörös, Narita and Bruno, ApJL 2014

Conclusions IV: twisted tubes & kink in the SW

Three from five tubes have the twist angle of $50^0 - 55^0$, which is less than the critical angle for the kink instability of the tubes with $M_A<0.5$. But it may become larger than the critical angle for tubes with $M_A>0.5$, therefore the magnetic reconnection can occur near boundary owing to kinking motion.

Suppose a magnetic flux tube is twisted with sub-critical angle near the Sun. The Alfvén Mach number can increase during the transport of the flux tube towards the Earth due to the decrease of the Alfvén speed.

Consequently, initially stable flux tube may become unstable to the kink instability at some distance from the Sun.

Kelvin-Helmholtz instability: external untwisted field

First we consider the situation when magnetic tubes move along the Parker spiral.

Therefore, the external magnetic field is axial.

Then we have the dispersion equation which is already presented above.

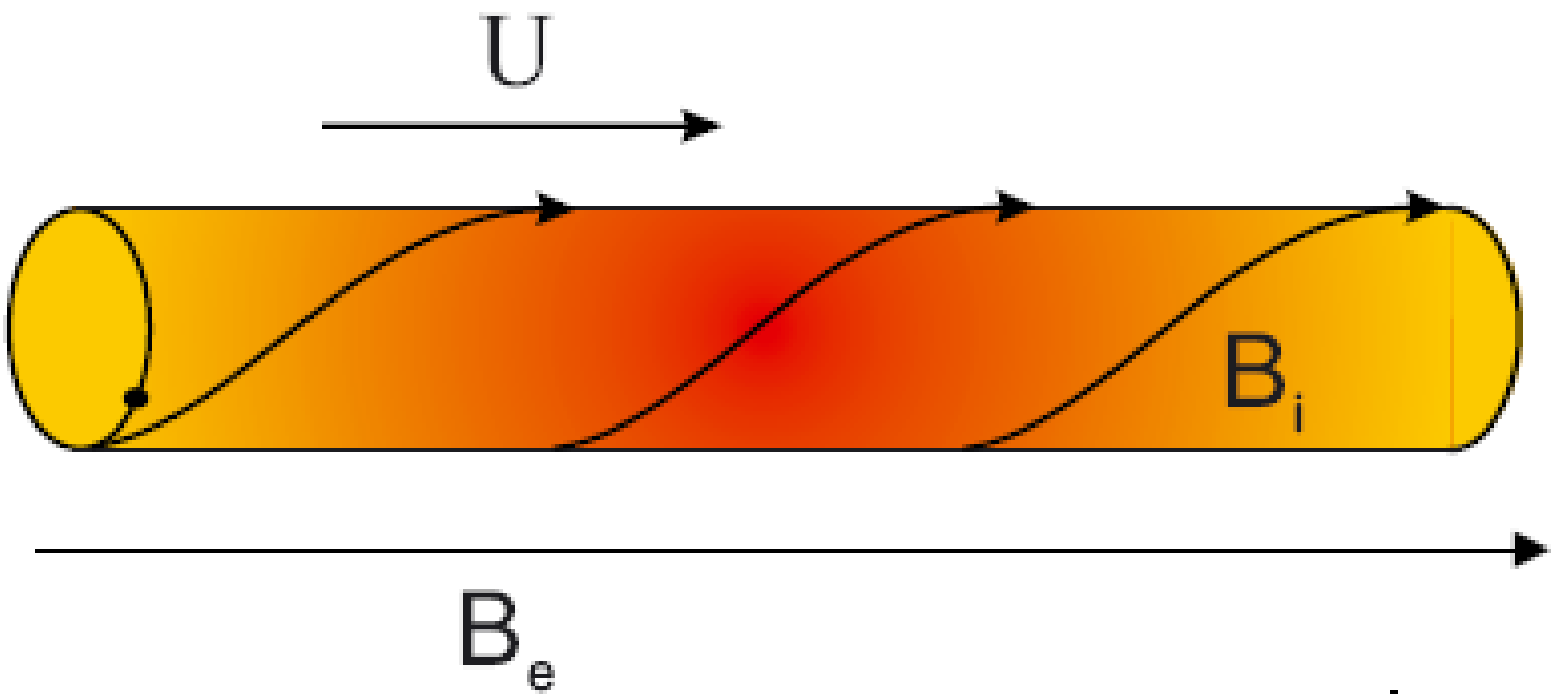

Kelvin–Helmholtz instability: external untwisted field

Thin flux tube approximation yields the polynomial dispersion relation

$$\omega^2 - \frac{2\rho_0 kU}{\rho_0+\rho_e}\omega + \frac{\rho_0}{\rho_0+\rho_e}\left(k^2U^2 - \omega_{A0}^2 + \omega_{Ae}^2\right)k^2U^2 - \frac{A^2\,|m|}{4\pi(\rho_0+\rho_e)} + \frac{2A\omega_{A0}\sqrt{4\pi\rho_0}}{4\pi(\rho_0+\rho_e)} = 0.$$

Let us consider the modes propagating perpendicular to magnetic field i.e. $\vec{k}\vec{B} \approx 0$.

Then we get

$$\omega^2 - \frac{2\rho_0 kU}{\rho_0+\rho_e}\omega + \frac{\rho_0}{\rho_0+\rho_e}\left(k^2U^2 + \omega_{Ae}^2\right)k^2U^2 - \frac{A^2\,|m|}{4\pi(\rho_0+\rho_e)} = 0.$$

The Kelvin-Helmholtz instability yields the complex frequency, therefore the instability criterion is

$$|m|\,M_A^2 > \left(1+\frac{\rho_0}{\rho_e}\right)\left(|m|\frac{B_e^2}{B_e^2}+1\right).$$

The criterion means that only super-Alfvénic motions are unstable as magnetic field stabilizes the Kelvin-Helmholtz instability.

Numerical solution of dispersion equation

The figure shows m = −3 unstable harmonics for different values of M_A after the solution of general dispersion equation.

It is seen that the critical Alfvén Mach number equals to 1.491 for m = −3 harmonics.

The analytically estimated critical Mach number is $M_A \approx 1.4907$ for m = −3 harmonics.

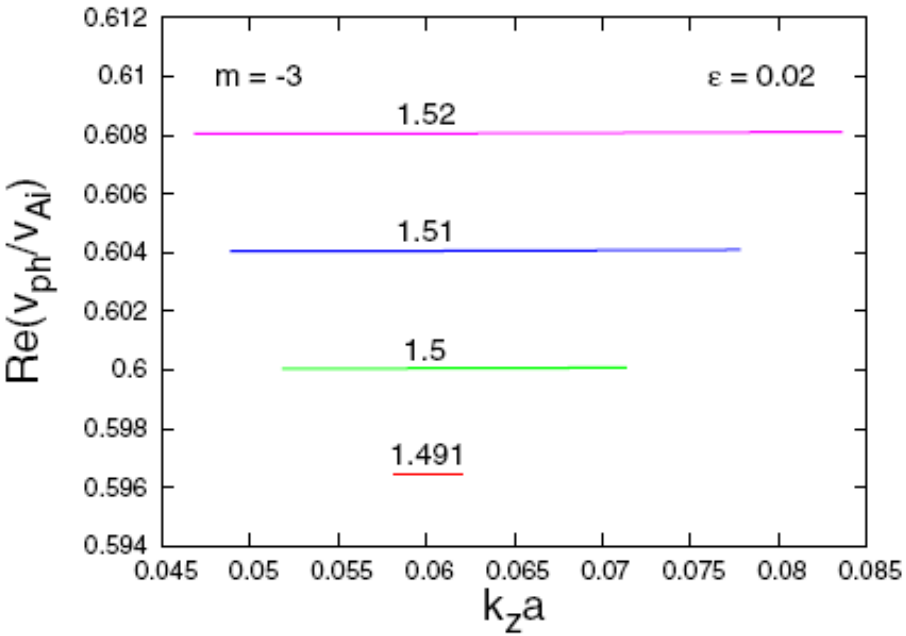

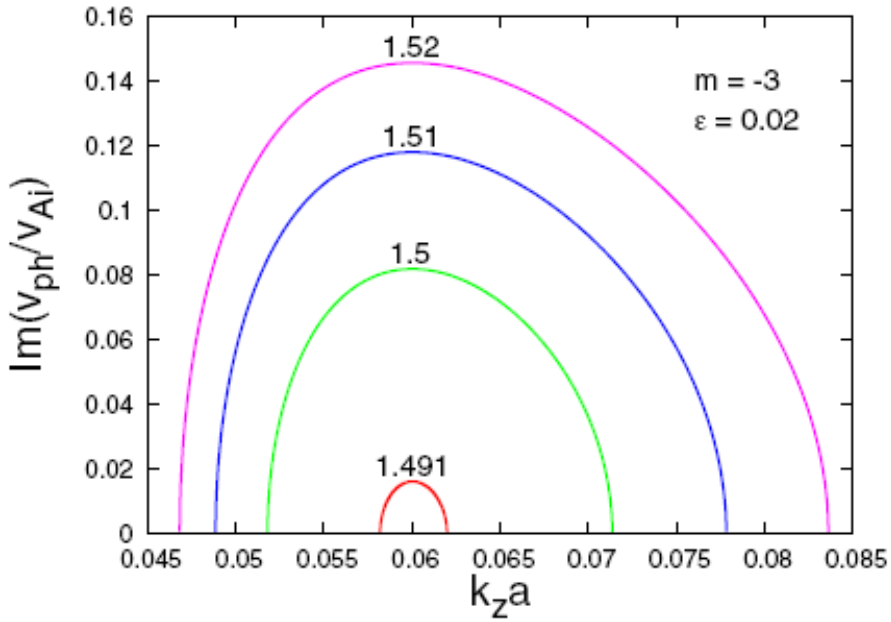

Zaqarashvili, Vörös and Zheliazkov, A&A, 2014

Kelvin-Helmholtz instability: external twisted field

If the tubes move at an angle to the Parker spiral, then the external magnetic field will have a transverse component.

Therefore, we now consider that the external magnetic field is also twisted and has a form

$$\left(0, B_{e\phi}\frac{a}{r}, B_{ez}\left(\frac{a}{r}\right)^2\right)$$

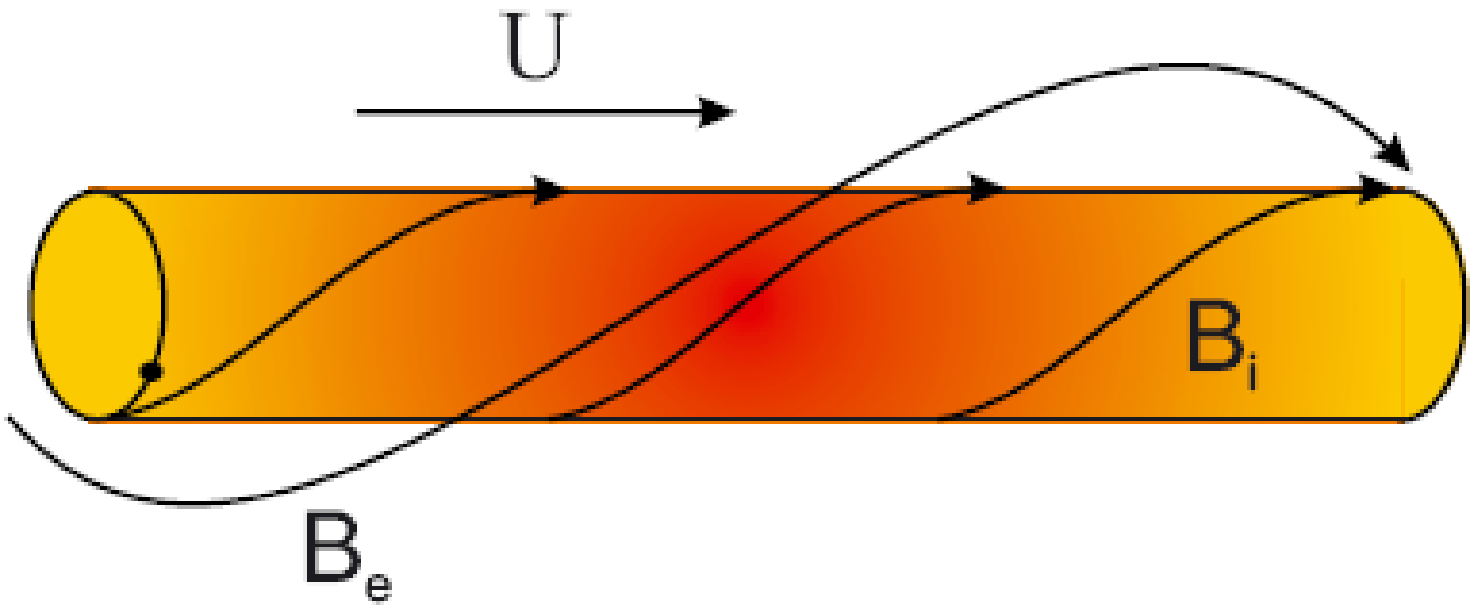

Kelvin-Helmholtz instability: external twisted field

The external density can be taken as

$$\rho = \rho_e \left(\frac{a}{r} \right)^4$$

so that the Alfvén frequency is constant

$$\omega_{Ae} = \frac{mB_{e\phi} + kaB_{ez}}{\sqrt{4\pi\rho_e a^2}} = const.$$

Then the solution of total pressure perturbation outside the tube is

$$p_t = a_e \frac{a^2}{r^2} K_\nu(m_e r),$$

where

$$m_e^2 = k^2 \left(1 - \frac{4B_{e\phi}^2 \omega^2}{4\pi\rho_e(\omega^2 - \omega_{Ae}^2)a^2} \right),$$

$$\nu = \sqrt{4 + m^2 - \frac{4m^2 B_{e\phi}^2}{4\pi\rho_e a^2 \left(\omega^2 - \omega_{Ae}^2\right)} + \frac{8mB_{e\phi}\omega_{Ae}}{\sqrt{4\pi\rho_e}\, a \left(\omega^2 - \omega_{Ae}^2\right)}}.$$

Kelvin-Helmholtz instability: external twisted field

The we get the following transcendental dispersion equation

$$\frac{\left((\omega - kU)^2 - \omega_A^2\right)F_m(m_0 a) - 2mA\omega_A / \sqrt{4\pi\rho_0}}{\rho_0\left((\omega - kU)^2 - \omega_A^2\right)^2 - 4\omega_A^2 A^2 / 4\pi} = \frac{\left[a^2\left(\omega^2 - \omega_{Ae}^2\right)Q_\nu(m_e a) - G\right]}{L - H\left[a^2\left(\omega^2 - \omega_{Ae}^2\right)Q_\nu(m_e a) - G\right]}.$$

Thin flux tube approximation yields the polynomial dispersion relation as

$$\left(1 + \frac{|m|}{2+|m|}\frac{\rho_e}{\rho_0}\right)\omega^2 - 2kU\omega + k^2U^2 - \frac{A^2 m}{4\pi\rho_e} = 0.$$

The Kelvin-Helmholtz instability yields the complex frequency, therefore the instability criterion is

$$|m| M_A^2 > 1 + \frac{2+|m|}{|m|}\frac{\rho_0}{\rho_e}.$$

Harmonics with sufficiently high m are always unstable for any value of M_A .

Kelvin–Helmholtz instability: external twisted field

The figure shows unstable harmonics for different values of M_A after the solution of dispersion equation.

It is seen that there are unstable harmonics with a sufficiently high azimuthal mode number m for any value of Alfvén Mach number.

Kelvin-Helmholtz vortices may contribute into the solar wind turbulence.

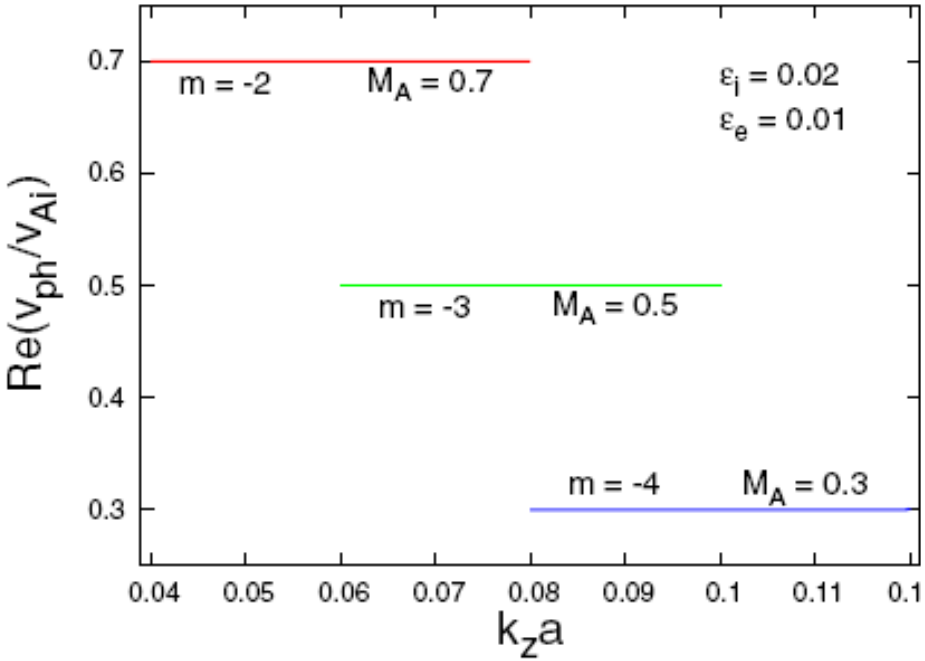

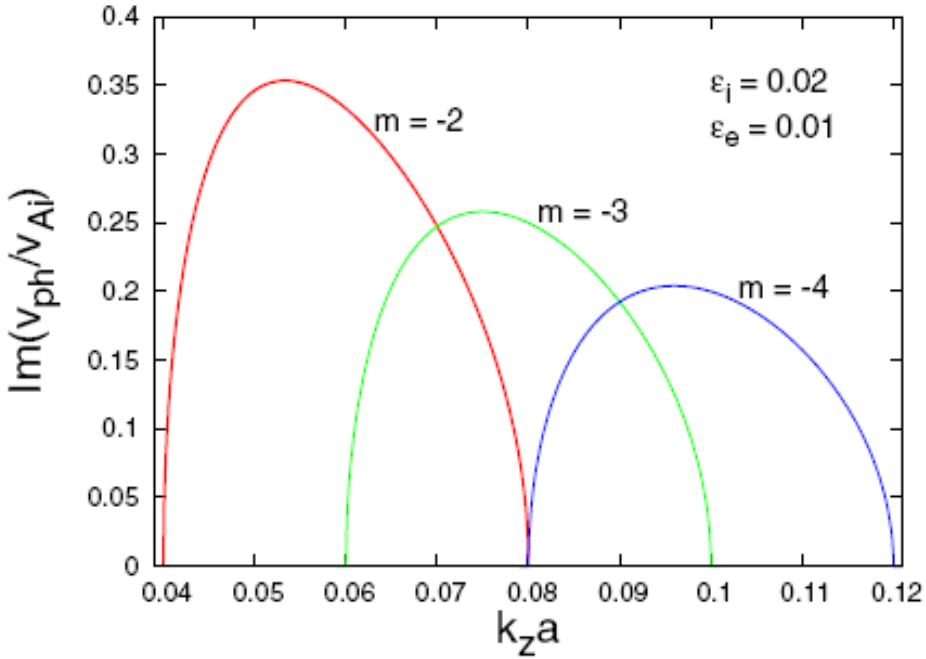

Zaqarashvili, Vörös and Zheliazkov, A&A, 2014

Conclusions V: Kelvin–Helmholtz instability

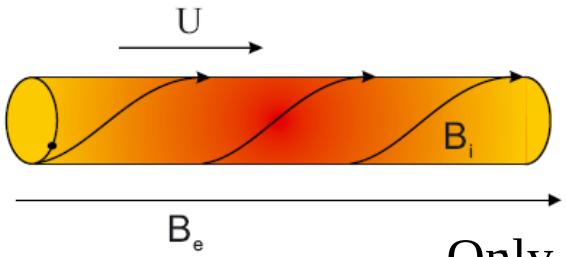

Instability criteria:

$$|m| M_A^2 > \left(1+\frac{\rho_0}{\rho_e}\right)\left(|m|\frac{B_e^2}{B_e^2}+1\right).$$

Only super-Alfvénic motions are unstable as magnetic field stabilizes the Kelvin-Helmholtz instability.

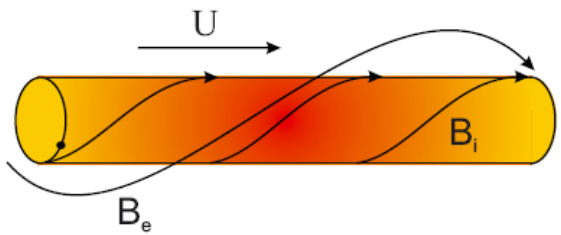

$$|m| M_A^2 > 1+\frac{2+|m|}{|m|}\frac{\rho_0}{\rho_e}.$$

Harmonics with sufficiently high m are unstable.

•Even slightly twisted magnetic tubes moving with an angle to the Parker spiral are unstable to the Kelvin-Helmholtz instability for sufficiently large azimuthal wave number - m.

•The Kelvin-Helmholtz vortices near the tube boundary may significantly contribute to solar wind turbulence.

Flux tubes within reconnection outflows

The 3D evolution of a guide field reconnection is dominated by the formation and interactions of twisted flux tubes (Daughton et al., 2011).

Moldwin et al. (1995,2000) suggested

reconnection ➔ flux tubes

Gosling (2013)

reconnection ➔ flux tubes

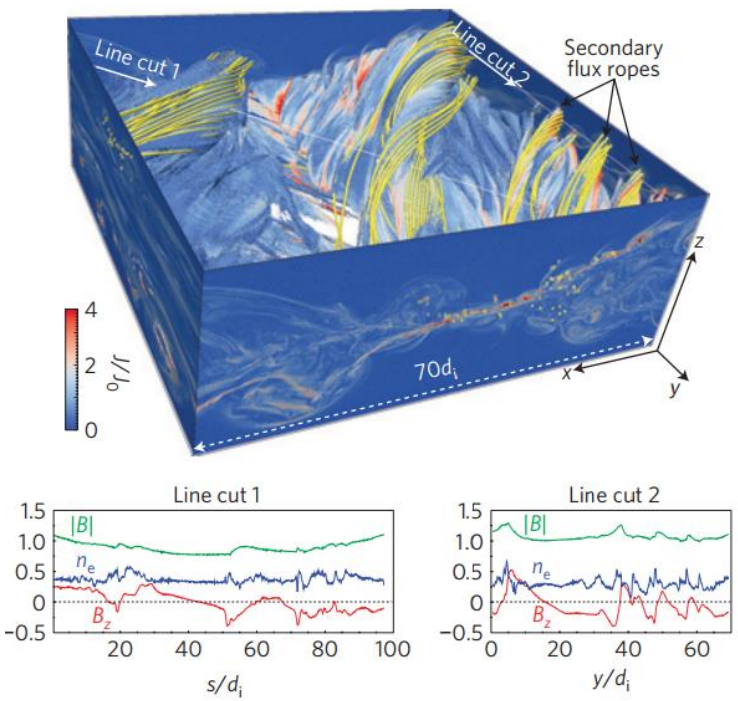

Kinetic simulations

Flux tubes within reconnection outflows

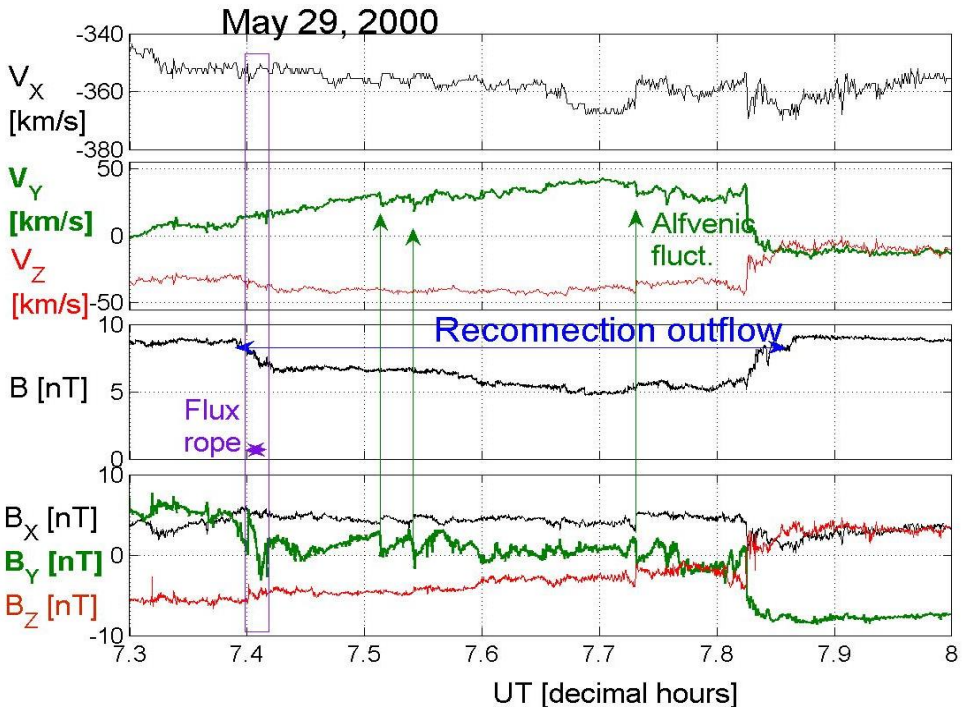

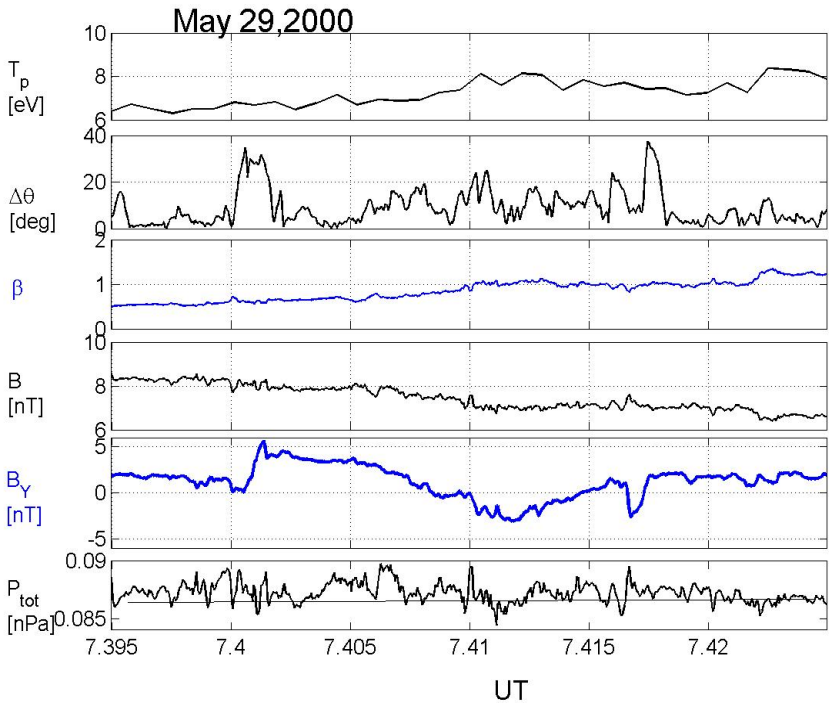

Non-force-free flux tube embedded in high-beta reconnection outflow.

In the Phan et al. (2009) reconnection database (51 events) we found 2 embedded flux tubes.

CONCLUSIONS

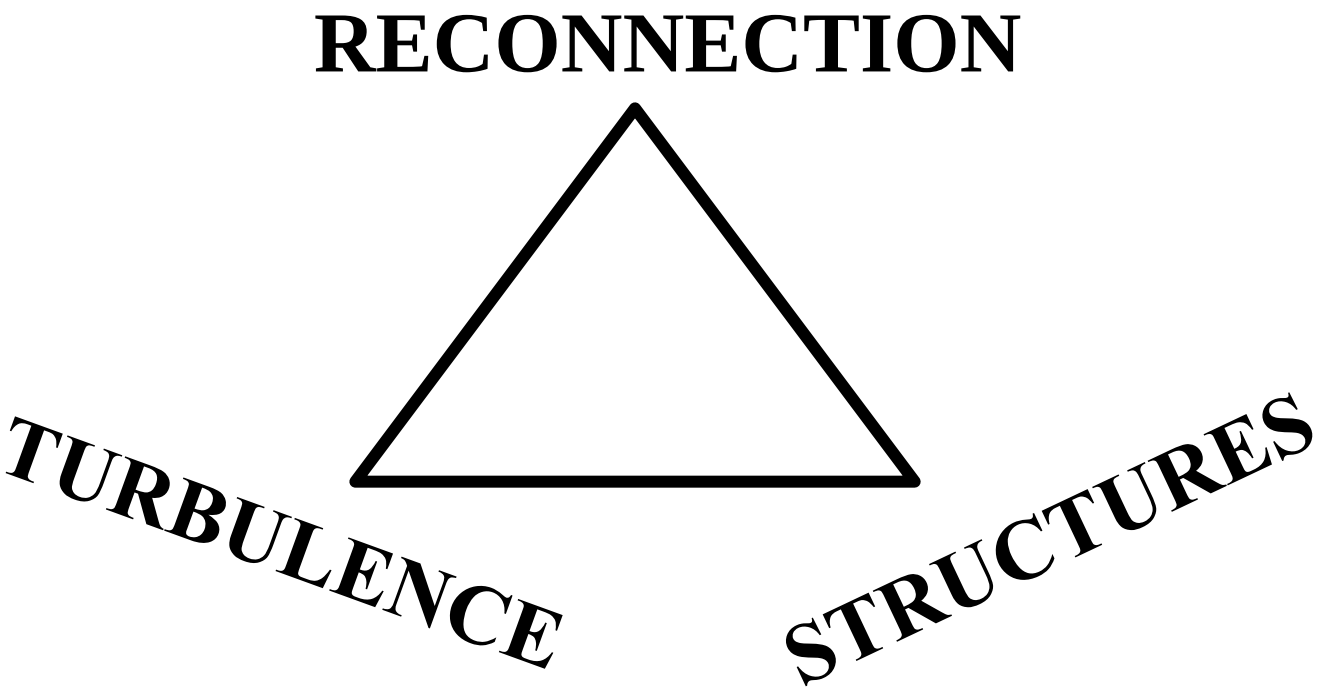

Radial evolution? Scales?
Occurrence frequency?
Heating?